5 Examination of Persistence Associated with Coupling

The results of Chapter 4 suggest that midlatitude air-sea interaction leads to increased persistence of atmospheric anomalies. In this chapter the increase in persistence is first documented and then the responsible mechanisms are examined in more detail. Model data are examined from the atmosphere, the surface mixed layer, and the deeper convective-diffusion portions of the ocean to document the characteristics of the persistence and to shed light on mechanisms that act to increase the persistence of climate variability in the coupled system. The vertical structure of ocean temperatures are analyzed using correlation, composite, and regression analysis to examine the role of submixed layer anomalies on the mixed layer. The influence of entrainment on ocean temperature anomalies is examined in a series of OWF experiments (see definition of OWF in Section 2-1), in which the MLM is forced with heat and momentum fluxes from the fully coupled simulation.

The examination of persistence is separated into two parts according to physical processes in order to begin to unravel the complex interactions that are taking place. First, the influence of entrainment of water from below the mixed-layer can have an impact on the variability and persistence of oceanic and atmospheric temperature anomalies (Figure 5-1) by changing the upper layer heat content through the transfer of mass and heat. Secondly, surface heat, momentum, and freshwater fluxes also change the variance and spectral characteristics of both the ocean and the atmosphere. Note that momentum only drives turbu-

lence and not currents in the MLM. Interactions at the surface of the ocean and the atmosphere are examined in Chapter 4 and also in Section 5.1.

The persistence of anomalies is documented in Section 5.1. Section 5.2 examines ocean temperature anomalies in the mixed layer and convective diffusive models. In Section 5.3 the role of entrainment on persistence is examined with a series of one-way forced sensitivity simulations. A summary is given in Section 5.4.

5.1 Persistence in the Atmosphere and Ocean

Visual inspection suggests that the time coefficients for the first EOF of seasonal (DJF) air temperature in the coupled simulation (Figure 4-11a) vary on longer time scales than those from the control simulation (Figure 4-11b). The autocorrelation of the time coefficients[1] of the dipole mode of variability of air temperature in the control and coupled simulations (Figure 5-2) confirms this observation. The persistence of the dipole mode of variability on interannual time scales has increased with coupling as seen in the larger autocorrelations of the time coefficients at lags of 1 and 2 years.

Thus far we have discussed the relationship between anomalies that are separated by an entire calendar year, which was artificially set by the EOF analysis. Two indices of monthly air temperature anomalies are constructed by averaging together model data at grid points in the northern and southern centers of the dipole mode of variability based on the EOF of air temperature (See Figure 5-3). Monthly autocorrelations of time series of these averages for both coupled and control simulations, shown in Figure 5-4, highlight possible differences between the southern and the northern part of the domain. In the northern part of the basin (Figure 5-4a), the autocorrelations decrease more slowly in the coupled simulation than the control. At a lag of about 10-11 months there is a notable increase in the autocorrelations of the coupled simulation over those from the control. There is also a small increase with lag in the autocorrelations of the control simulation at a lag of about 12

1. Note that the lag is in years since the EOF is calculated using wintertime averaged (December to February) air temperature.

months. Note that the time coefficients of EOF1 for wintertime (DJF) are also significantly autocorrelated at a lag of one year (Figure 5-2) in the coupled simulation. In addition, autocorrelations of total surface heat fluxes (not shown) from the control simulation in the northern part of the domain are weakly positive (0.2-0.3) between one winter and the next. This suggests that there is some degree of persistence already in the control simulation.

In the southern part of the domain, autocorrelations decrease more slowly with lag in the coupled than in the control simulation (Figure 5-4b). The most notable difference is at a lag of approximately 5 months, when the control autocorrelation is slightly negative and the coupled autocorrelation has plateaued at a small positive value. The decrease of autocorrelations between the coupled and control simulations appears to be smaller in the north than the south: persistence in the anomalies in the north is enhanced more with coupling.

The seasonal variation of the persistence of anomalies is examined by constructing autocorrelations that begin at each of the months of the year for monthly lags. Autocorrelations that begin in March (Figure 5-5a) can account for the small peak at around 10-11 months seen in Figure 5-4a in the autocorrelations including all 12 months in the coupled simulation. In the autocorrelations of air temperature in the southern part of the domain that begin in March (Figure 5-5b) there is no peak at 10-12 months. In the southern part of the domain the monthly autocorrelations in the coupled simulation are stronger than the control for lags up to four months (Figure 5-5b).

These autocorrelation plots (Figure 5-2 to Figure 5-5) indicate an increase of persistence of air temperature anomalies on the interannual and monthly time scales.

5.1.1 Namias and Born 'Re-emergence' Mechanism

The statistically significant autocorrelation in the northern part of the domain between air temperature in March and air temperature 10-11 months later may be explained by the 'Re-emergence' or 'Namias and Born' hypothesis (Namias and Born, 1970 and 1974). Ocean temperature anomalies that exist during late winter when the mixed layer is deep are sequestered below the shallow stable summer mixed layer. In the subsequent fall months as the mixed layer deepens, the temperature anomalies from the previous winter are reincorporated into the mixed layer. A modeling and observational study by Alexander and Deser (1995) at northern midlatitude ocean weathership stations strongly supports the 'Re-emergence' mechanism.

A summary of monthly autocorrelations of air temperature starting at all months in the northern part of the domain for the control and coupled simulations (Figure 5-6a and b) shows the dominance of the winter to winter correlations over other quasi-annual correlations. Correlations larger than 0.36 are statistically significant at the 95% or greater level. The seasonal distribution of autocorrelations shown in Figure 5-6 are noisy and somewhat confusing but are included to highlight several points. The autocorrelations in the control simulation are weaker than those in the coupled simulation, with many more regions of small correlations. The correlations between one winter and the following winter in the coupled simulation (starting months of February to April) stand out in Figure 5-6 and are the largest autocorrelations (0.4-0.6) found during the year at a lag of about 10-12 months. Autocorrelations of observed air temperature (constructed in a parallel manner as the model autocorrelations) in the northern part of the domain (Figure 5-6c) closely resemble those from the coupled simulation and display large positive autocorrelations between air temperature during winter and that at a lag of 7-9 months. The observed correlations are smaller than those in the model, suggesting that the model over represents this process. Processes such as advection due to Ekman effects, not included in the ocean model, influence ocean temperatures in nature. The large autocorrelations (0.4 to 0.6) from winter to winter in the coupled simulation tilt with a slope of approximately minus one month per one month lag.

This indicates that winter air temperature during January to April is most strongly correlated with air temperature the following January, which suggests that the seasonal cycle plays an important role in the ‘re-emergence’ mechanism. Additionally, the autocorrelations for shorter time scales in the coupled simulation decay more slowly then those in the control simulation during the summertime (May to August). The summertime autocorrelations will be discussed further later in this section.

The most notable changes with coupling at shorter time lags occurs in both the northern and the southern domains with a shift in the 0.4 autocorrelation time from a lag of ~2 months to ~3 months (Figure 5-6 and Figure 5-7). As seen in the autocorrelations of air temperature for the southern grid points during March (Figure 5-5b), the autocorrelation from early spring to the following winter is not significant. The observed autocorrelations in the southern part of the domain display weak correlations from one winter to the next (Figure 5-7c), in agreement with the coupled simulation.

Autocorrelations of MLM ocean mixed layer temperature (Figure 5-8) are consistent with the air temperature autocorrelations. In the northern part of the basin there are significant autocorrelations (Figure 5-8a) between ocean temperature during winter of one year and that the following winter. This is not evident in the ocean temperature autocorrelations for southern part of the domain (Figure 5-8b). The autocorrelations of observed SST (Figure 5-8c and d) are consistent with those of observed air temperature, with strong (weak) autocorrelations of SST from one winter to the next in the north (south). Significant negative correlations exist between ocean temperature during one winter and total heat flux the following winter (Figure 5-9). The evidence suggests that re-emergence is primarily responsible for the persistence in ocean temperature anomalies seen at lags of 10-12 months. In the southern part of the basin, significant autocorrelations from one winter to the next do not occur in model or in the observations.

5.1.2 Decreased Damping by Heat Fluxes

The largest increases with coupling of monthly autocorrelations of air temperature take

place for autocorrelations that begin during the summer months in the northern part of the domain. This is evident from comparing coupled and control autocorrelations for all months of air temperature in the northern part of the domain (Figure 5-6a and b) around a lag of 2 months. The autocorrelations that begin in July for air temperature averaged over the northern and southern grid points are shown in Figure 5-10. There is a large increase in the persistence of air temperature anomalies in the northern part of the domain and a moderate increase in the south. A likely mechanism for this increase in persistence clearly visible during the warmer months of the year is associated with changes in 'Thermal Damping' (Hasselmann, 1976; Frankignoul, 1985; Barsugli, 1995) as a result of coupling. This is not to say that changes in 'Thermal Damping' do not operate during the winter months in this model, but just that it is more clearly seen in the warmer months. Turbulent heat fluxes act to strongly damp air temperature anomalies when the ocean temperatures do not vary (Frankignoul, 1985). In the coupled simulation, ocean temperatures respond to atmospheric anomalies and consequently the damping by heat fluxes of atmospheric anomalies decreases (decreased 'Thermal Damping'). This mechanism suggests that once the atmosphere sets up a particular anomaly pattern, interaction with the ocean helps to sustain these climate anomalies.

The analysis of winter data in Chapter 4 showed an increase in seasonal (DJF) variance of air temperature with a concurrent decrease in the variability of heat fluxes. These changes in variability are consistent with a decrease in 'Thermal Damping' (Barsugli, 1995), suggesting that it operates during the wintertime.

The evidence for a decrease in thermal damping is more evident in summer than winter. The ratio of coupled over control standard deviation of seasonally averaged (Figure 5-11a) and monthly (Figure 5-11b) summer (June to August) air temperatures indicate an increase of variability with coupling. There is a larger increase in the summer seasonal variance (Figure 5-11a) than in the monthly variance (Figure 5-11b) with coupling.

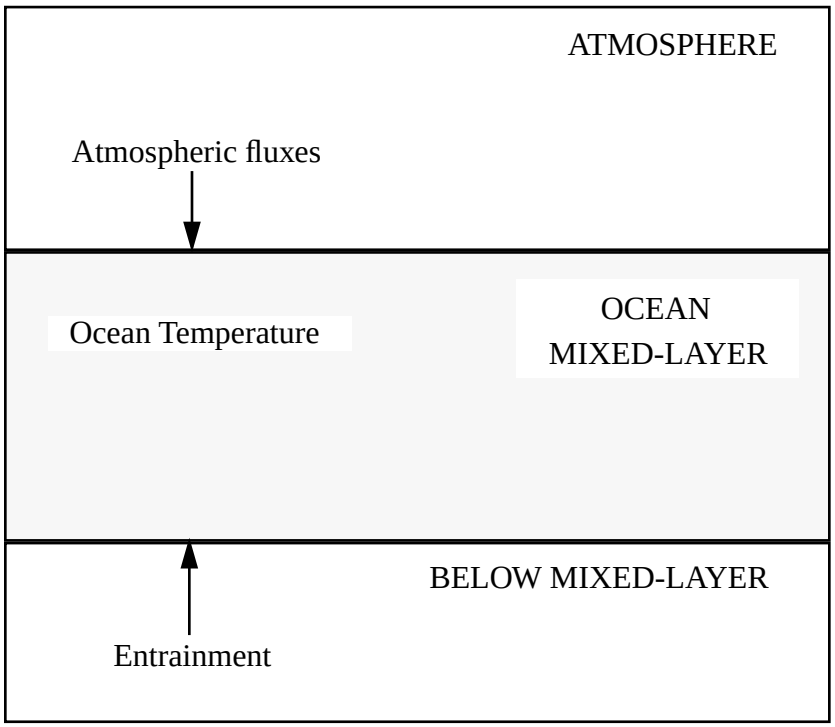

Figure 5-1. Schematic depicting the surfaces of interaction in the coupled model setup. Mixed layer properties are a function of entrainment from below the mixed layer and air-sea interaction at the atmosphere-ocean interface.

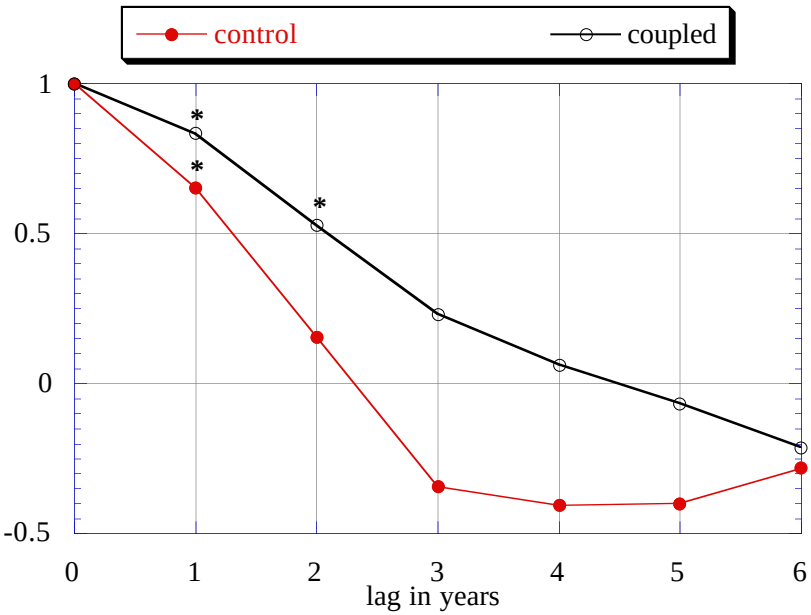

Figure 5-2. Autocorrelation of the time coefficients of EOF1 (based on an averaged DJF anomalies) of T_{air} from the control (dashed line) and the coupled (solid line) simulations. Statistical significance is indicated by a '*' and the lag is in years.

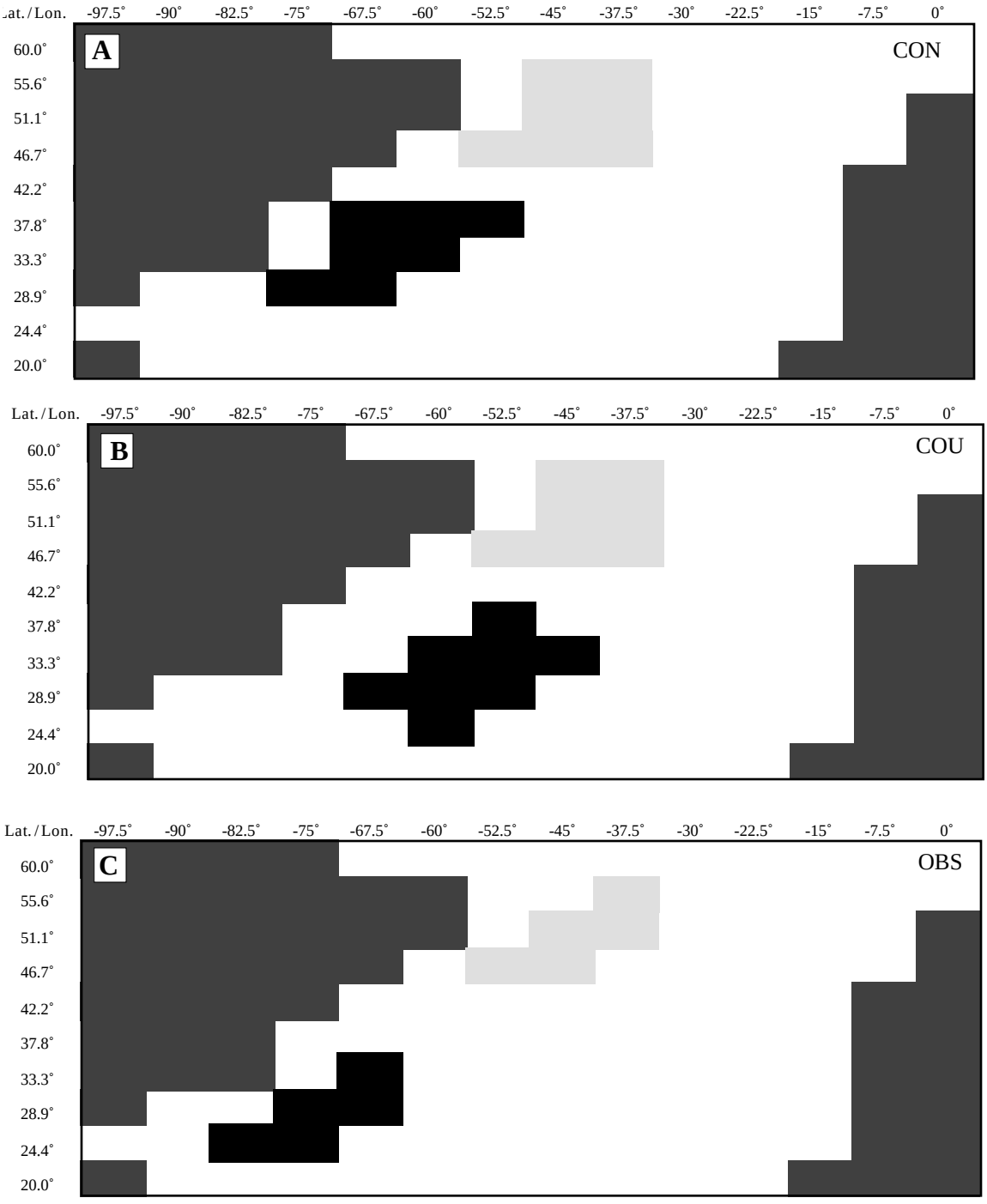

Figure 5-3. Schematics outlining regions that display the largest variability in the dipole mode of air temperature in the northern (dotted) and southern (black) regions of the North Atlantic in the a) control simulation, b) coupled simulation, and c) observations (COADS). Data is averaged over these grids boxes to construct time series.

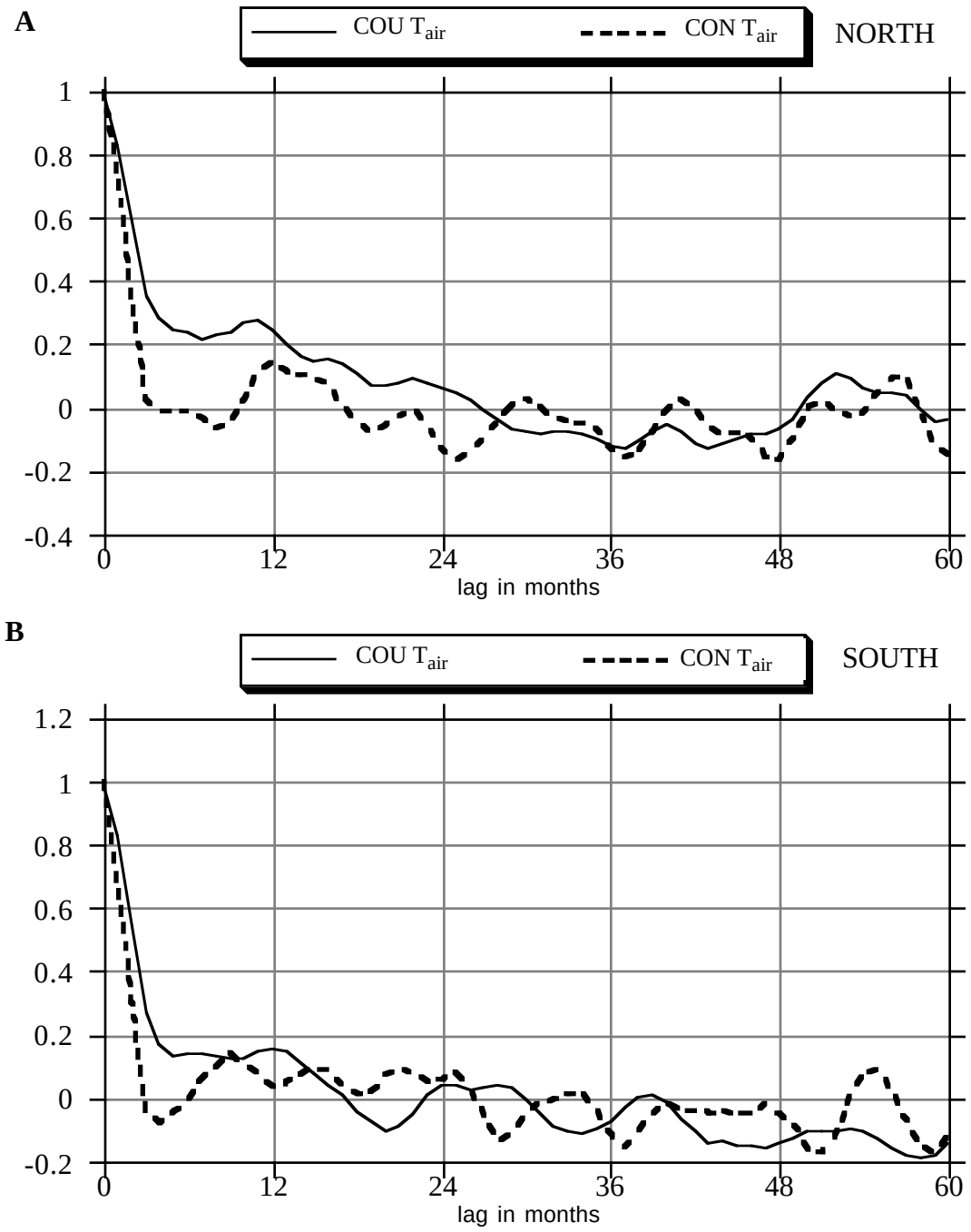

Figure 5-4. Autocorrelations of air temperature for all months using time series averaged over grid points in the a) northern and b) southern regions of the dipole domain for the coupled (solid) and control (dashed) simulations. Correlations larger than .11 are statistically significant at the 95% level or greater.

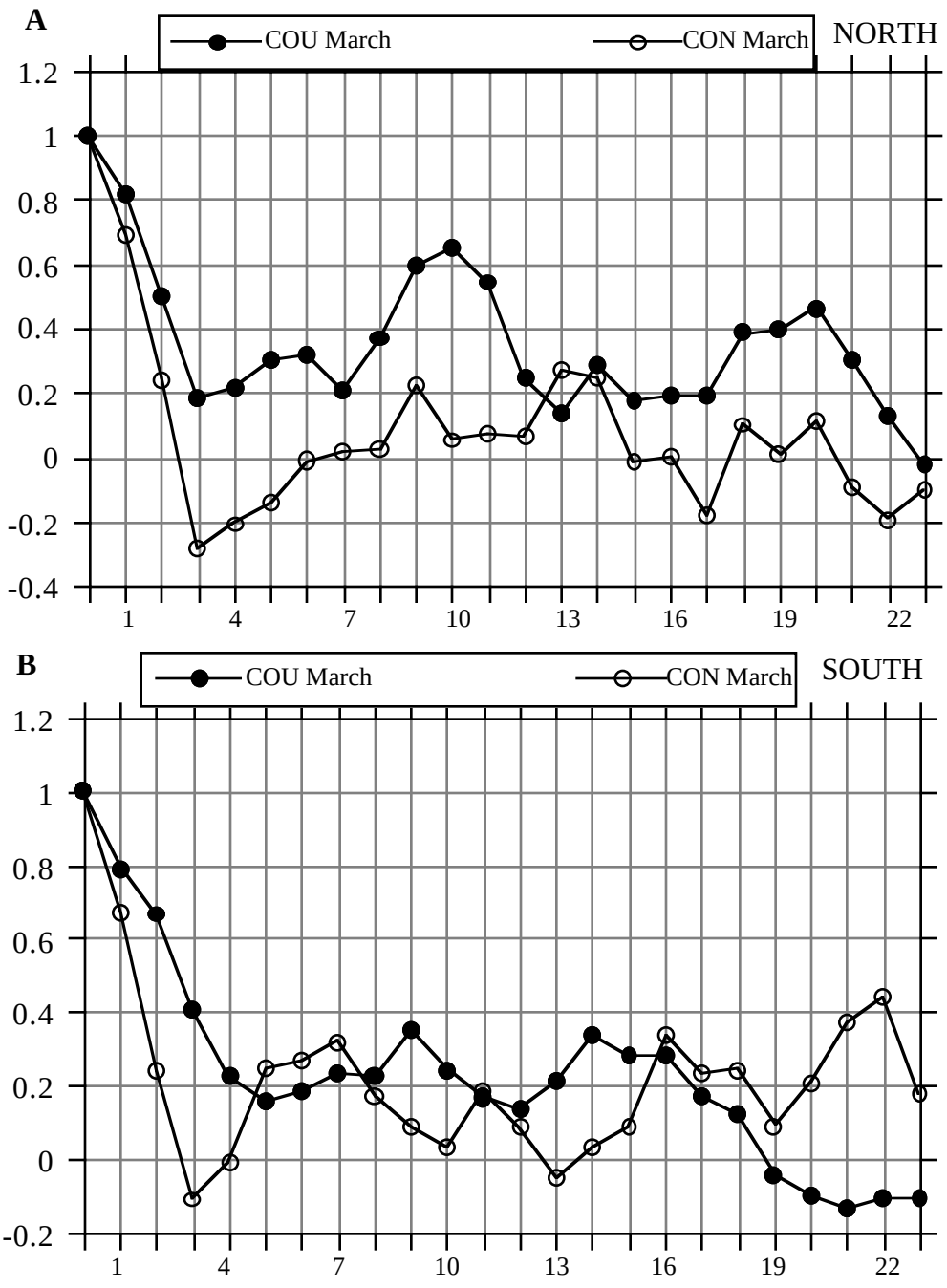

Figure 5-5. Autocorrelations of air temperature that begin in March for a) the northern and b) southern parts of the domain. The x-axis represents the number of months after March. The autocorrelations from the coupled simulation are indicated by the solid dot and from the control simulations by circles. Autocorrelations greater than 0.36 are statistically significant at the 95% or greater level, as determined from Student's t-test.

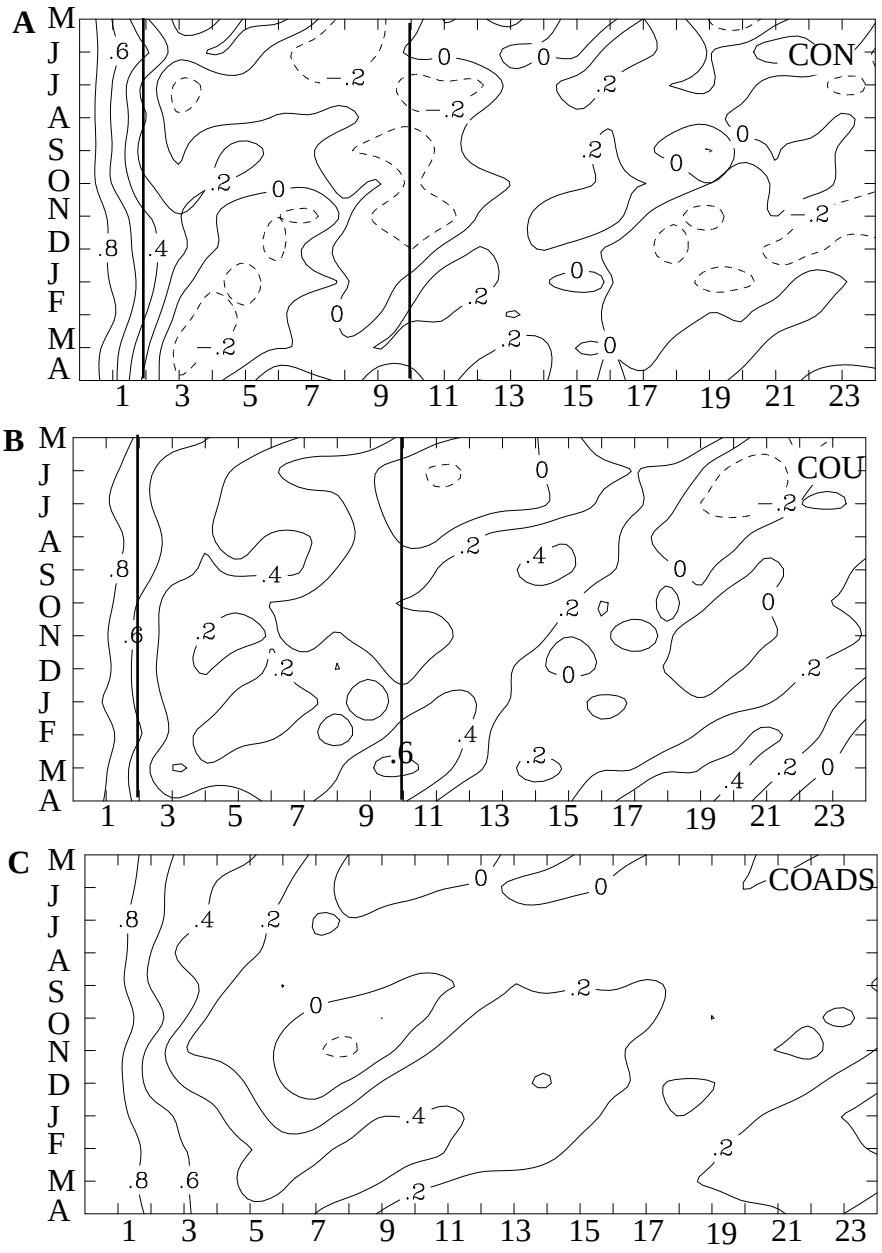

Figure 5-6. Monthly autocorrelations of T_{air} in the northern part of the domain for the a) control, b) coupled, c) observed. The starting months are shown on the ordinate. Autocorrelations greater than 0.36 are statistically significant at the 95% or greater level, as determined from Student's t-test. At the top left corner, the ordinate begins with the month of May and continues down the column until April. The numbers spanning from 0 to 24 on the x-axis indicate the number of months after the starting month, which is given by values on the y-axis. Note that Figure 5-10a is a horizontal cross-section taken at March of the plots in Figure 5-6. The vertical lines at 2 and 10 months highlight the monthly and interannual time scales of persistence, respectively

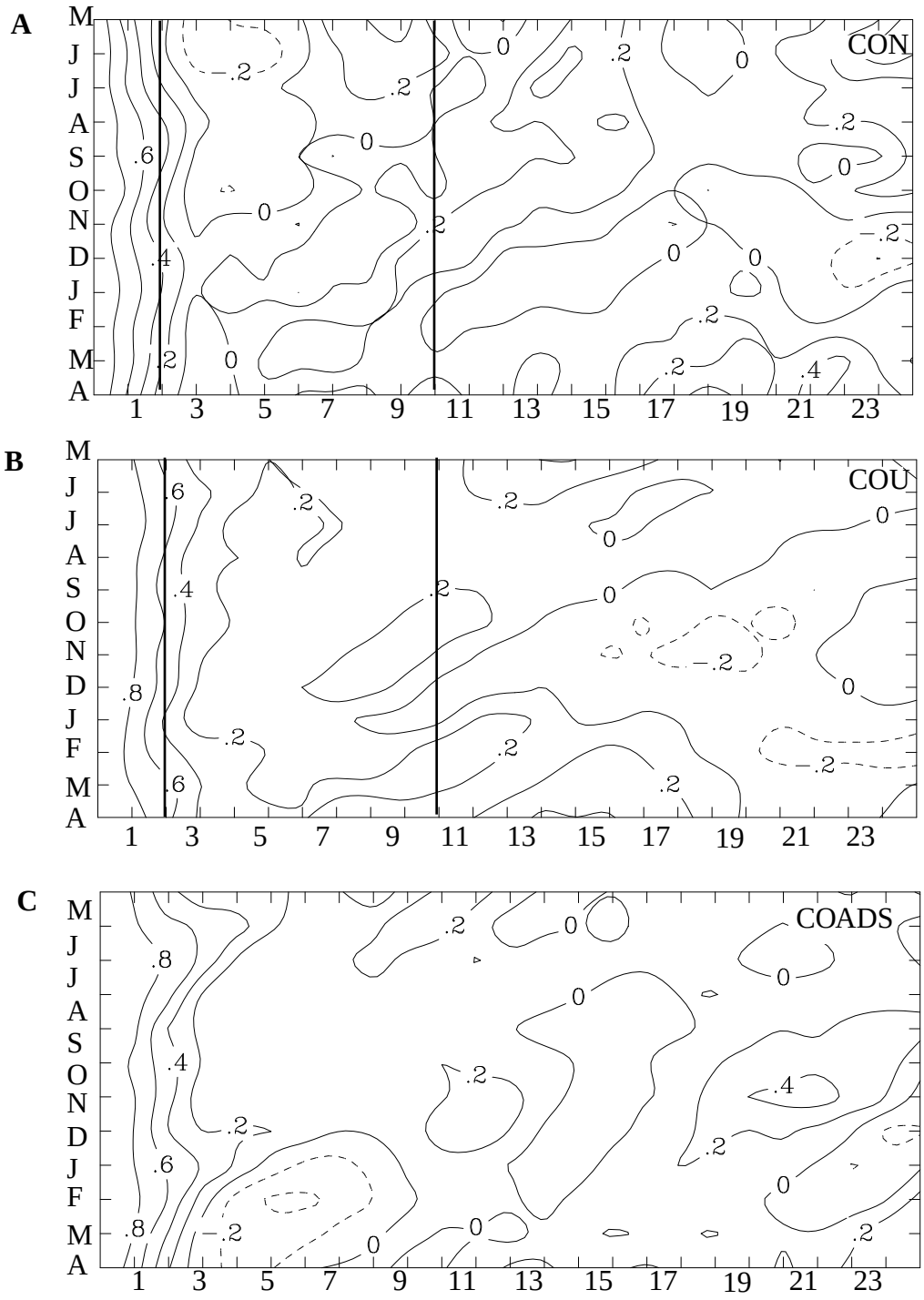

Figure 5-7. Monthly autocorrelations of T_{air} in the southern part of the domain for the a) control, b) coupled, c) observed. The starting months are shown on the ordinate. Autocorrelations greater than 0.36 are statistically significant at the 95% or greater level, as determined from Student's t-test.

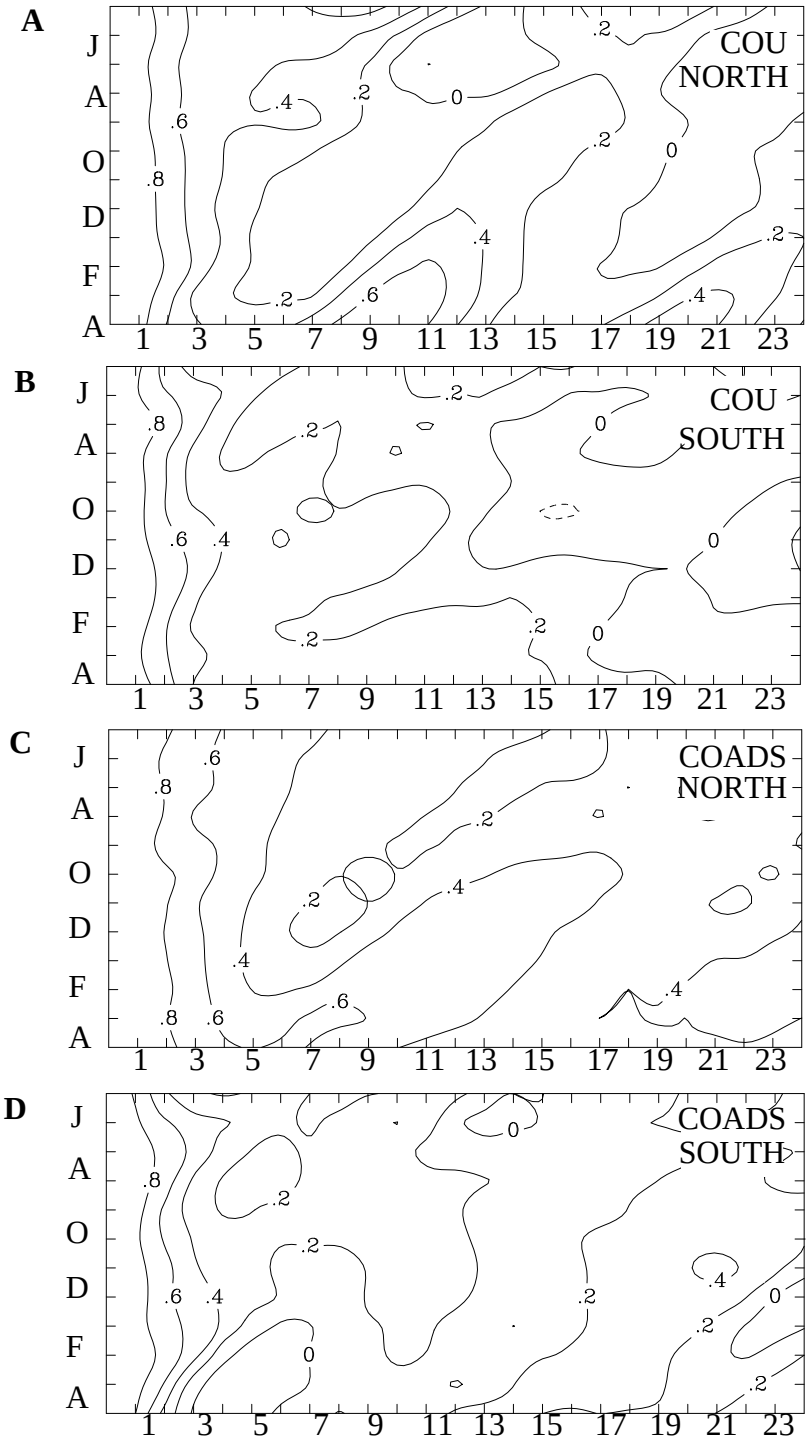

Figure 5-8. Monthly autocorrelations of T_{mix} (SST) from the a) northern coupled, b) southern coupled, c) northern observed, and d) southern observed data set. The starting months are shown on the ordinate. Autocorrelations greater than 0.36 are statistically significant at the 95% or greater level, as determined from Student's t-test.

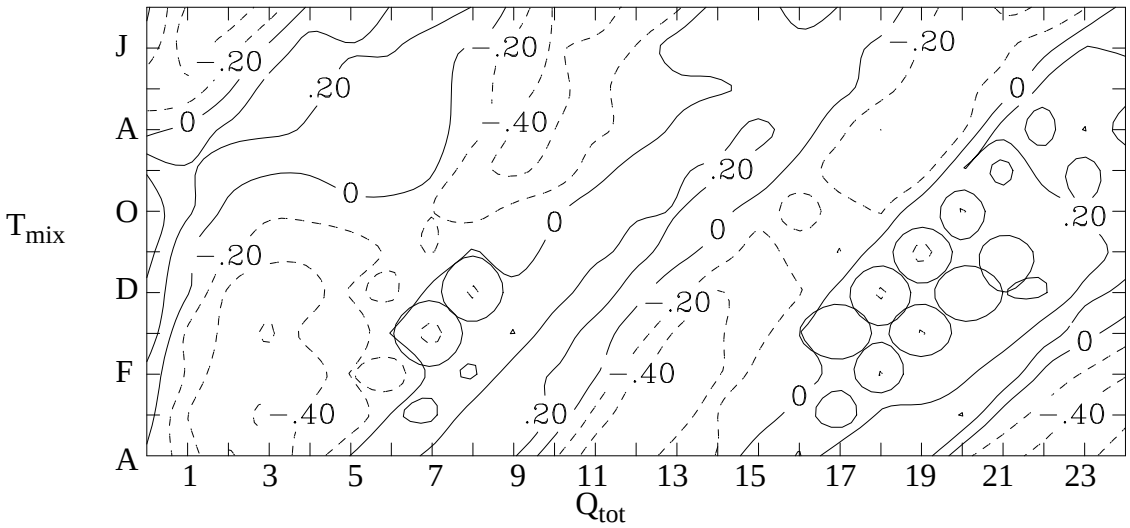

Figure 5-9. Monthly lag correlations between T_{mix} and Q_{tot} in the northern part of the ocean domain. The starting months are shown on the ordinate. Autocorrelations greater than 0.36 are statistically significant at the 95% or greater level, as determined from Student's t-test.

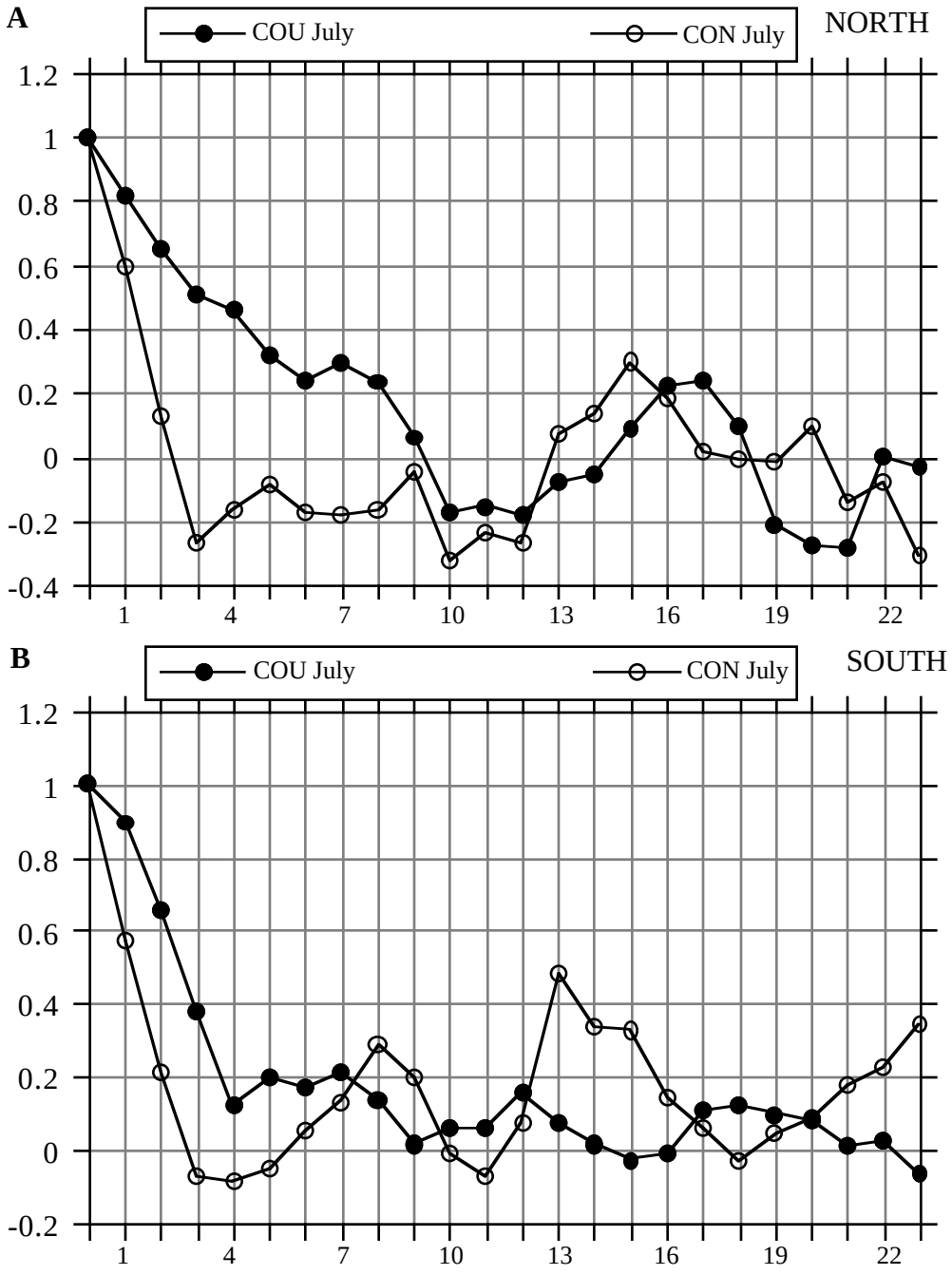

Figure 5-10. Autocorrelations of air temperature that begin in July for a) the northern and b) southern parts of the domain. The x-axis represents the number of months after July. The autocorrelations from the coupled simulation are indicated by the solid dot and from the control simulations by circles. Autocorrelations greater than 0.36 are statistically significant at the 95% or greater level, as determined from Student's t-test.

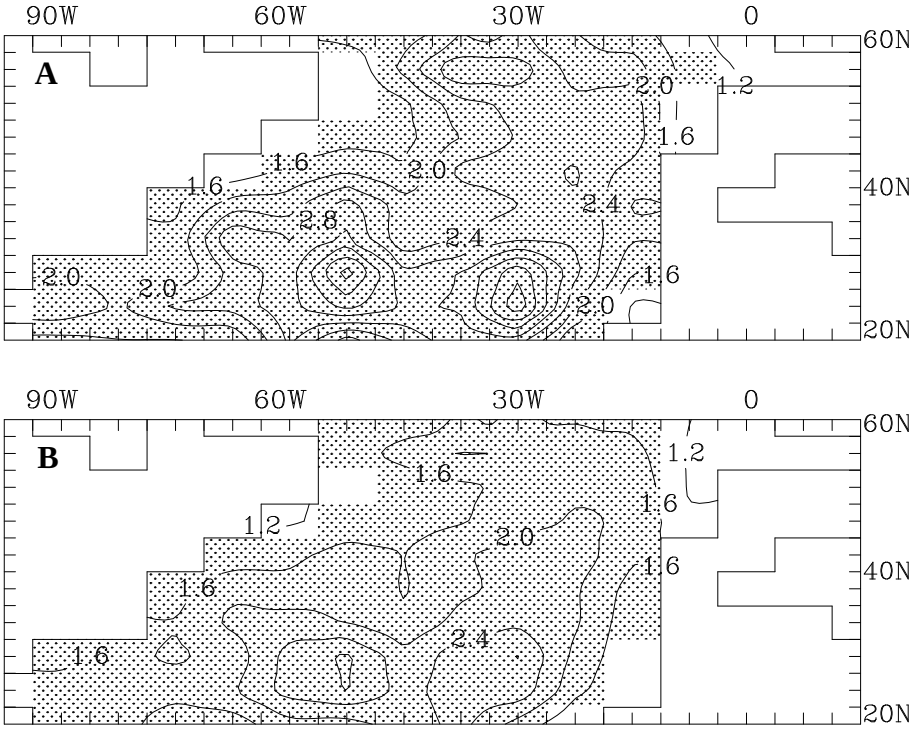

Figure 5-11. Ratio of coupled over control standard deviation of air temperature for a) seasonal anomalies and b) monthly anomalies during June to August. Shading indicates statistical significance at the 95% level or greater using an F-test.

5.2 Vertical Structure of Oceanic Variability

The vertical structure of ocean temperature anomalies from the coupled simulation are examined in this section. The mean ocean temperature structure for the top 225 meters for the northern grid points (Figure 5-12a) reaches its maximum of 15 ˚C during August and minimum of 7-8 ˚C during January-April. Maximum (minimum) mean mixed layer depths (Figure 5-12a) are reached during February (June-July). In the southern part of the domain (not shown) the maximum temperature of 27 ˚C is also reached in August while minimum temperatures of 19-20 ˚C are reached in January-March. Figure 5-12b demarcates the northern and southern grid points used to make the area averages discussed in this section. The mean annual cycle of mixed layer depths in the south (not shown) is similar to that in the north except that in the south the mixed layer depth shallows faster during March and April.

Ocean temperatures anomalies from the surface to a depth of 225 meters from May of year 12 to April of year 31 are examined in this section. Data from the first 11 years of the coupled simulation are unfortunately unavailable due to technical difficulties. Monthly anomalies are calculated with respect to the mean of the 20 monthly values. This is in contrast to mixed layer and atmospheric variables, whose monthly means are based on 31 years of model data. Displayed in Figure 5-13 are the monthly anomalies of ocean temperature averaged over the northern grid points, where the mixed layer ocean temperature variability is largest in the northern center of the dipole pattern. The largest and deepest anomalies generally occur during the winter months and propagate slowly downward for several years until they are replaced with anomalies of the opposite sign. The period of anomalously cold ocean temperatures during years 12-17 corresponds to positive time coefficients of EOF1 of air temperature (Figure 4-11a), which represent negative air temperature anomalies. Similarly, the anomalously warm ocean temperatures seen during years 22-27 are associated with warm air (negative time coefficients, Figure 4-11a). The MLM predicted mixed layer depths are shown as a heavy line in Figure 5-13. An example of the recurrence mechanism can be seen at the end of year 23 through year 24 in the vertical temperature anom-

alies (Figure 5-13). Anomalies are large 0.8˚C during winter of year 23 at the surface of the ocean, the anomalies are seen at depth during the summer of year 24 and the re-emergence of anomalies is evident into the mixed layer during fall.

Ocean temperature anomalies over the center of the southern lobe of the dipole (see Figure 5-3) penetrate to similar depths as those in the north but are smaller in magnitude by approximately 50% (30%) for positive (negative) anomalies (not shown). Southern temperature anomalies are largely opposite in sign to those in the north, which is consistent with the analysis of surface fields (Chapter 4).

The correlations of surface ocean temperature and the *concurrent* temperatures with depth display a strong seasonal cycle (Figure 5-14a and b) in the northern and southern domains. Correlations are large with depth during the winter months when mean mixed layers are deep and entrainment mixing is active. Summer and fall surface temperatures are anticorrelated with those deeper than 70 (155) meters in the northern (southern) part of the domain. It is not known to what extent the summer anomalous gradient is important for the winter anomalies that follow in the northern part of the domain. The stable mixed layer reforms closer to the ocean surface during the warm season leaving anomalies from the winter below the mixed layer. The anomalies in the surface layer in summer are associated with the overlying atmospheric anomalies and anticorrelated with ocean temperature anomalies below 60 meters.

Correlations between February ocean surface temperatures and those at the surface for the subsequent 13 months decrease during the warm months and increase again during the following winter (December to February) for both the northern and southern parts of the domain (Figure 5-15). The correlations in the north are larger (0.7-0.8) the following winter (December to March) than those in the south (0.3-0.4). Regression coefficients (not shown) of winter ocean temperature on ocean temperature for the previous February are 0.7-0.8 (0.2-0.3) ($^{\circ}C\ ^{\circ}C^{-1}$) in the northern (southern) part of the domain. This suggests that the influence of anomalous entrainment from one winter to the next is stronger in the north than in the southern part of the domain. One needs to exercise caution since the autocorrelation

of the time coefficients of air temperature of EOF1 in the control simulation are significant at a lag of one year, therefore, the strong correlations from February to the next winter in the north could simply be due to atmospheric and land influences. In the control simulation, the autocorrelation for total heat flux (Q_{tot}) starting in March reaches a maximum of 0.3 at a lag of 9 months in the north and 0.4 at a lag of 11 months in the south (Figure 5-16a and b). The CCM1 control simulation exhibits low frequency variability, which could amplify the re-emergence mechanism. The autocorrelations of total heat flux (Q_{tot}) around a lag of 12 months are nearly equal in the southern and northern parts of the domain, suggesting that the re-emergence is not primarily associated with persistence that is part of the natural variability of the atmospheric model. Lag/lead correlations with a base point at a depth of 37.5 meters during August, which is below the summer mixed layer, are shown in Figure 5-17. In the north, the submixed layer temperatures during August are significantly correlated with ocean temperatures from the previous and following winters and are weakly correlated with concurrent ocean surface temperatures. The correlation pattern is similar in the south as that just described in the north except the correlations are overall weaker. The carryover from one winter to the next is somewhat stronger in the north than the south.

Composites for the available warm (19, 22, 23, 24, 25) and cold (12, 13, 15, 29, 30) winters for ocean temperature are constructed by averaging those winters with peaks in the time coefficients of the first EOF of mixed layer temperature. Note that these warm and cold composite winters are based on peaks in the time coefficients of EOF1 of mixed layer temperature, which tend to lag the peaks in the time coefficients of EOF1 of air temperature by one year. Warm and cold composites for the subsurface temperature anomalies in the north are shown in Figure 5-18, with the peak wintertime (Dec. to Feb.) values at the center of each plot. The composites in Figure 5-18 suggest that temperature anomalies are reincorporated in to the mixed layer during the fall and winter after the peak winter. In the southern part of the domain (not shown) for the both cases the conclusions are similar as in the north but for the cold case (anomalies are warm in the south) the anomalies are very weak in the south. Since the re-emergence mechanism appears largest after the peak in

EOF1 of air temperatures, the re-emergence of ocean temperature anomalies acts to persist the air temperature anomaly pattern.

Collectively, we find that temperature anomalies during late winter are sequestered below the shallow summer mixed layer and reenter the surface layer in the fall to impact the ocean temperature anomalies in the surface layer. The analysis of ocean temperature anomalies with depth supports the idea that the ‘Re-emergence’ mechanism explains the persistence of anomalies from one winter to the next. This is consistent with the lag autocorrelations of air and ocean temperature in the northern and southern centers of the dipole discussed in Section 5-1. Ocean temperatures below the mixed layer are significantly correlated from late winter to the following fall and these correlation patterns are consistent with the ‘Re-emergence Mechanism’.

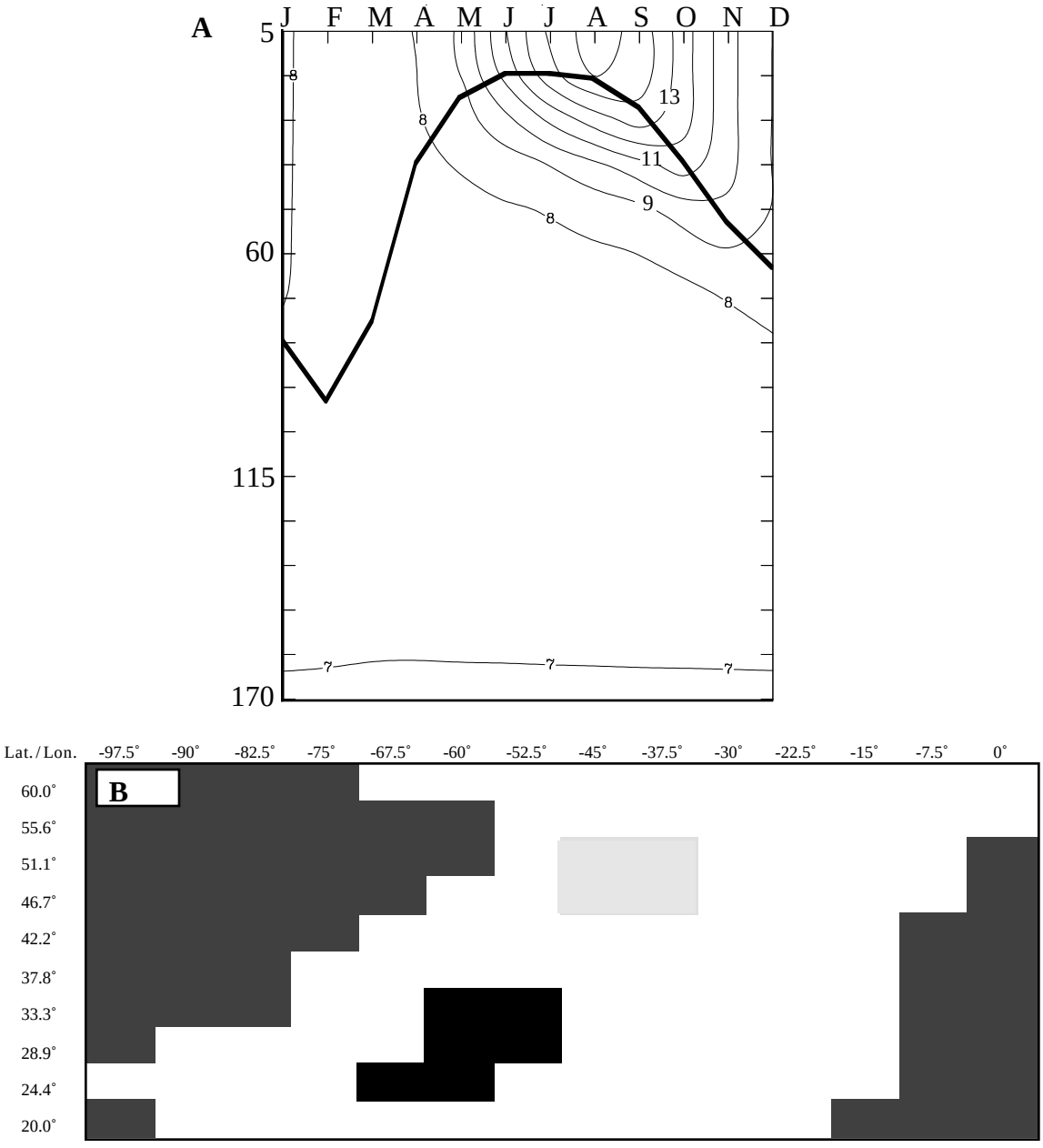

Figure 5-12. Panel a) Mean annual cycle of coupled model temperature in ˚C with depth averaged over the northern grid points. Climatological mixed layer depth, as predicted by the MLM, is represented by the heavy line. Panel b) represents the grid boxes used to construct the area averages of the model data in the northern and southern parts of the North Atlantic domain.

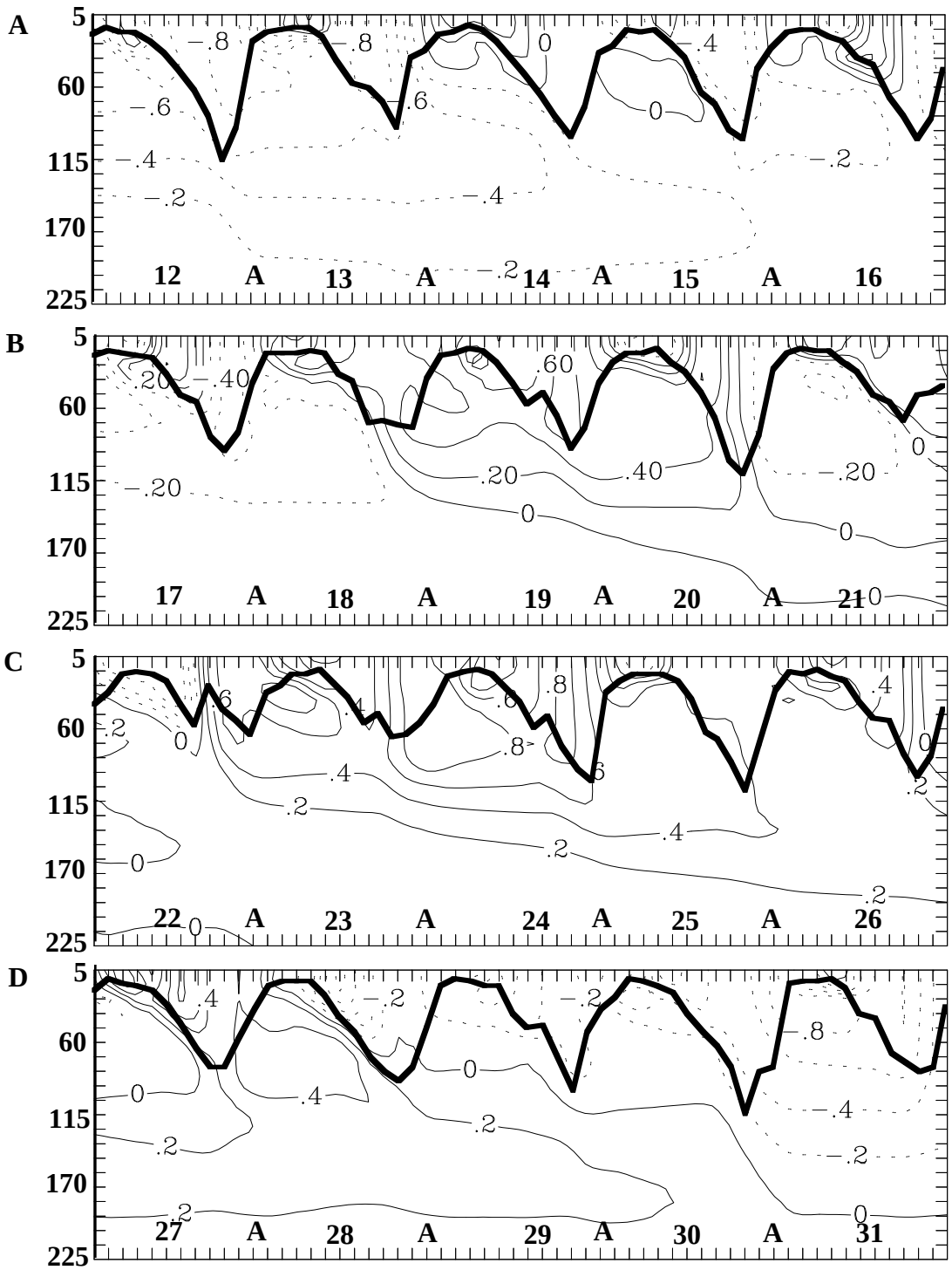

Figure 5-13. Monthly subsurface ocean temperature anomalies in the north beginning in May for coupled model years a) 12-16, b) 17-21, c) 22-26, and d) 27-31 in ˚C. 'A' marks the month of April such that the first 'A' in panel a is from year 12. Depth is in meters and each tick is 11 meters. The heavy line represents the model predicted mixed layer depth.

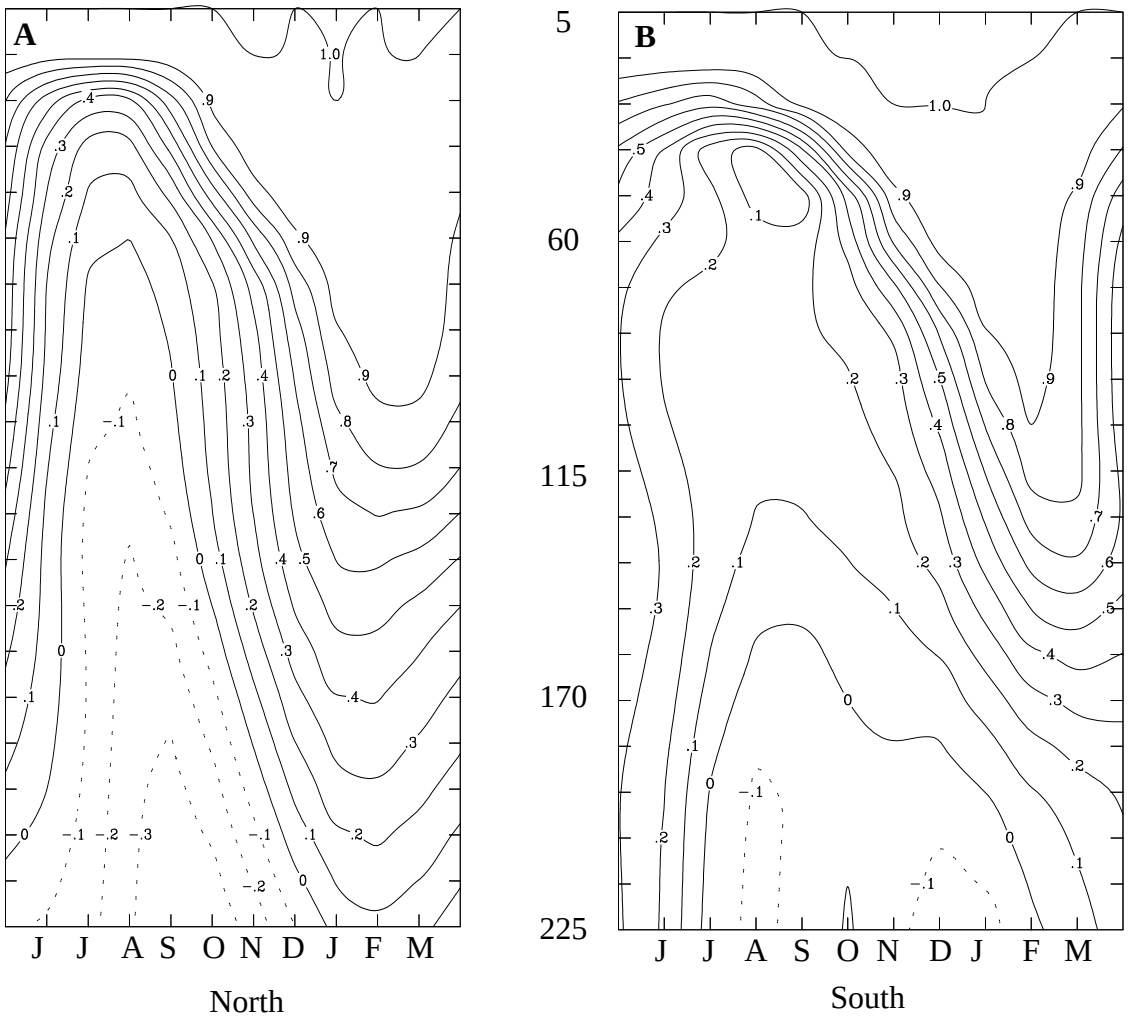

Figure 5-14. Correlations between surface ocean temperature and *concurrent* subsurface temperatures from May to April for grid points averaged over the north and south.

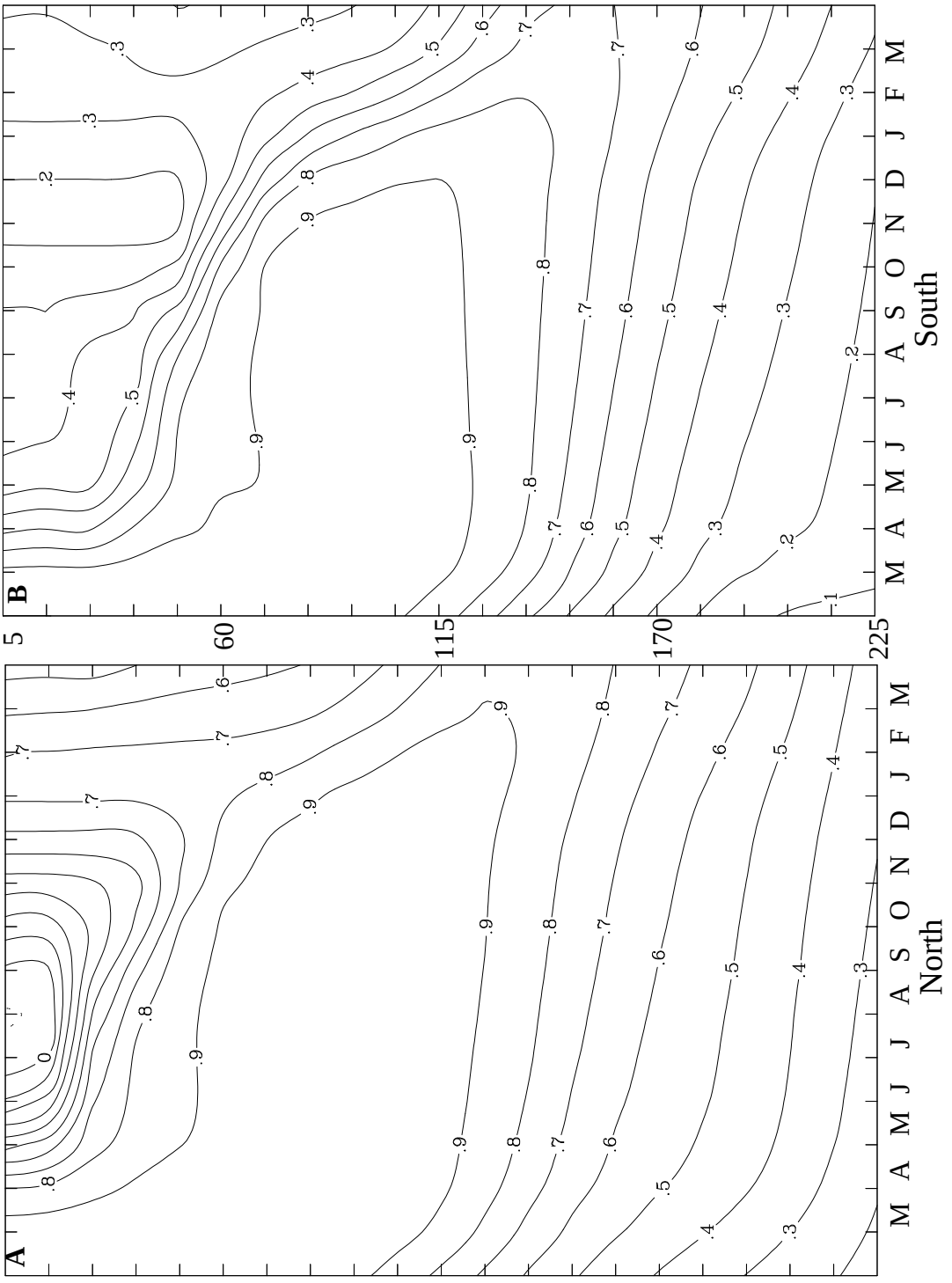

Figure 5-15. Correlations between February surface ocean temperature and ocean temperatures from the surface to a depth of 225 meters for the next 14 months. The average of northern (southern) grid points is shown in panel a (b).

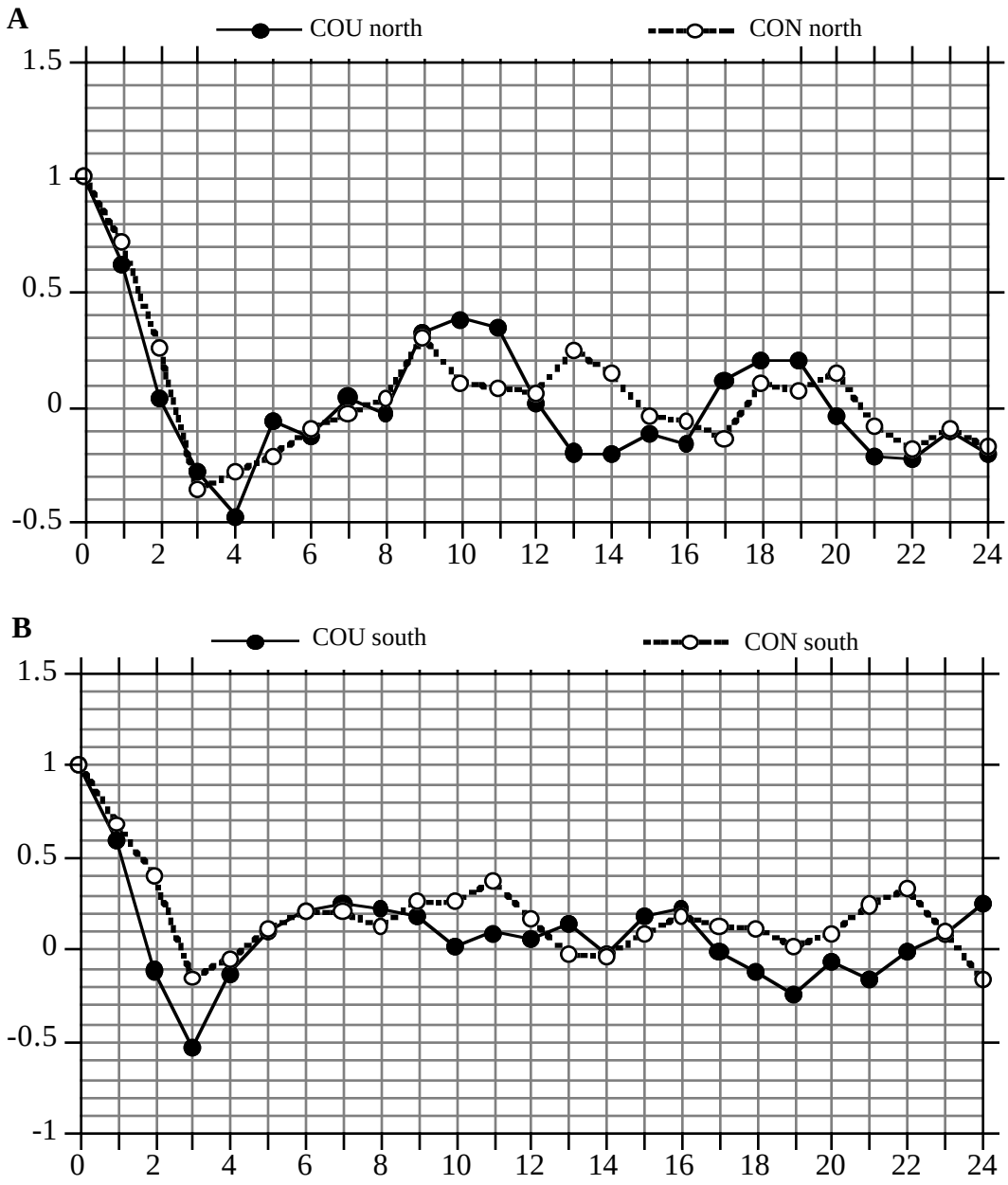

Figure 5-16. Autocorrelations of total heat flux that begin in March for a) the northern and b) southern parts of the basin. The abscissa represents the number of months after March. The autocorrelations from the coupled simulation are indicated by a solid dot and the control by circles. Autocorrelations greater than 0.36 are statistically significant at the 95% or greater level, as determined from Student's t-test.

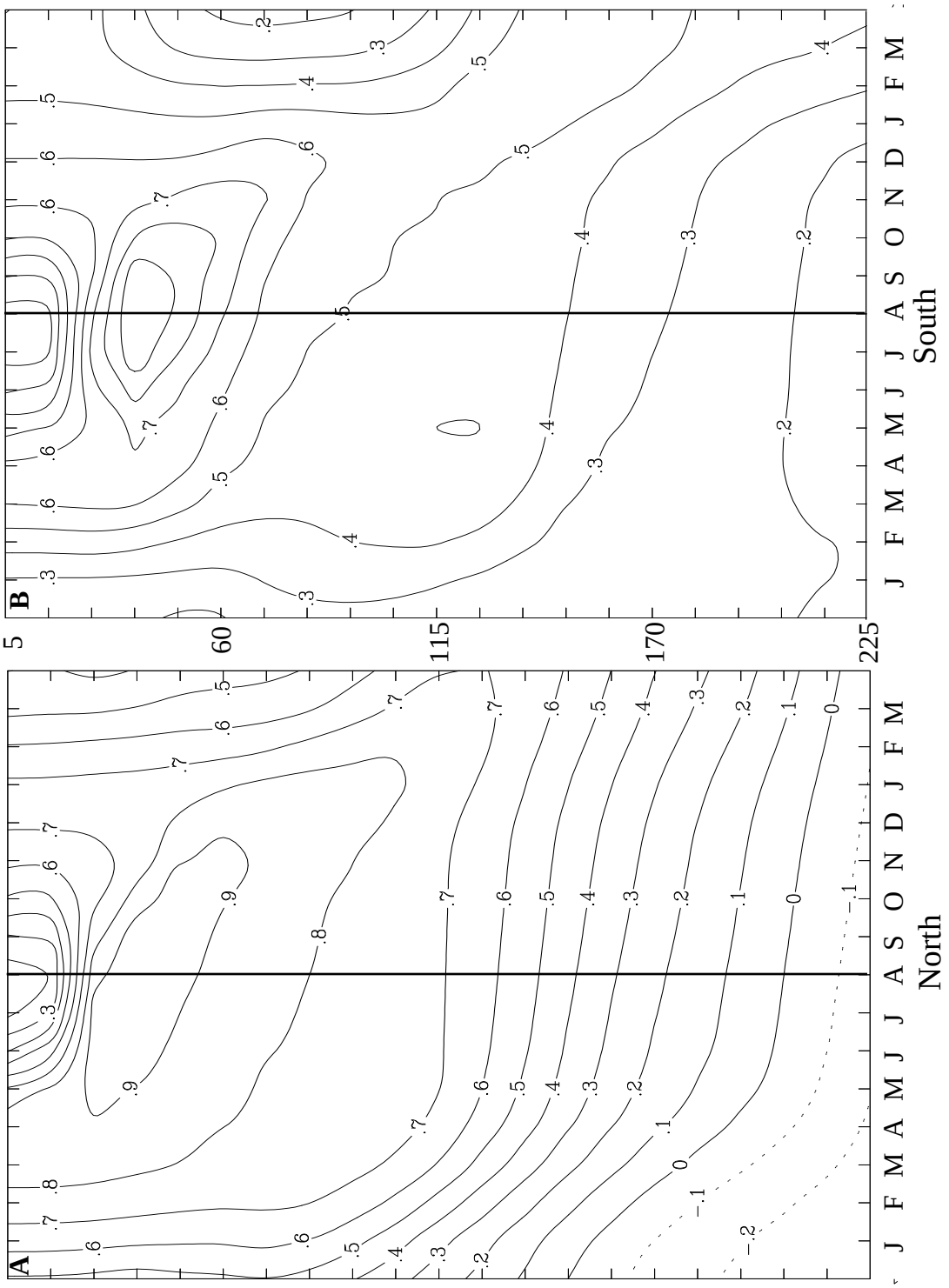

Figure 5-17. Correlations between August ocean temperature at 37.5 meters and ocean temperature from the surface to 225 meters during the previous and following 8 months. The average of northern (southern) grid points is shown in panel a (b).

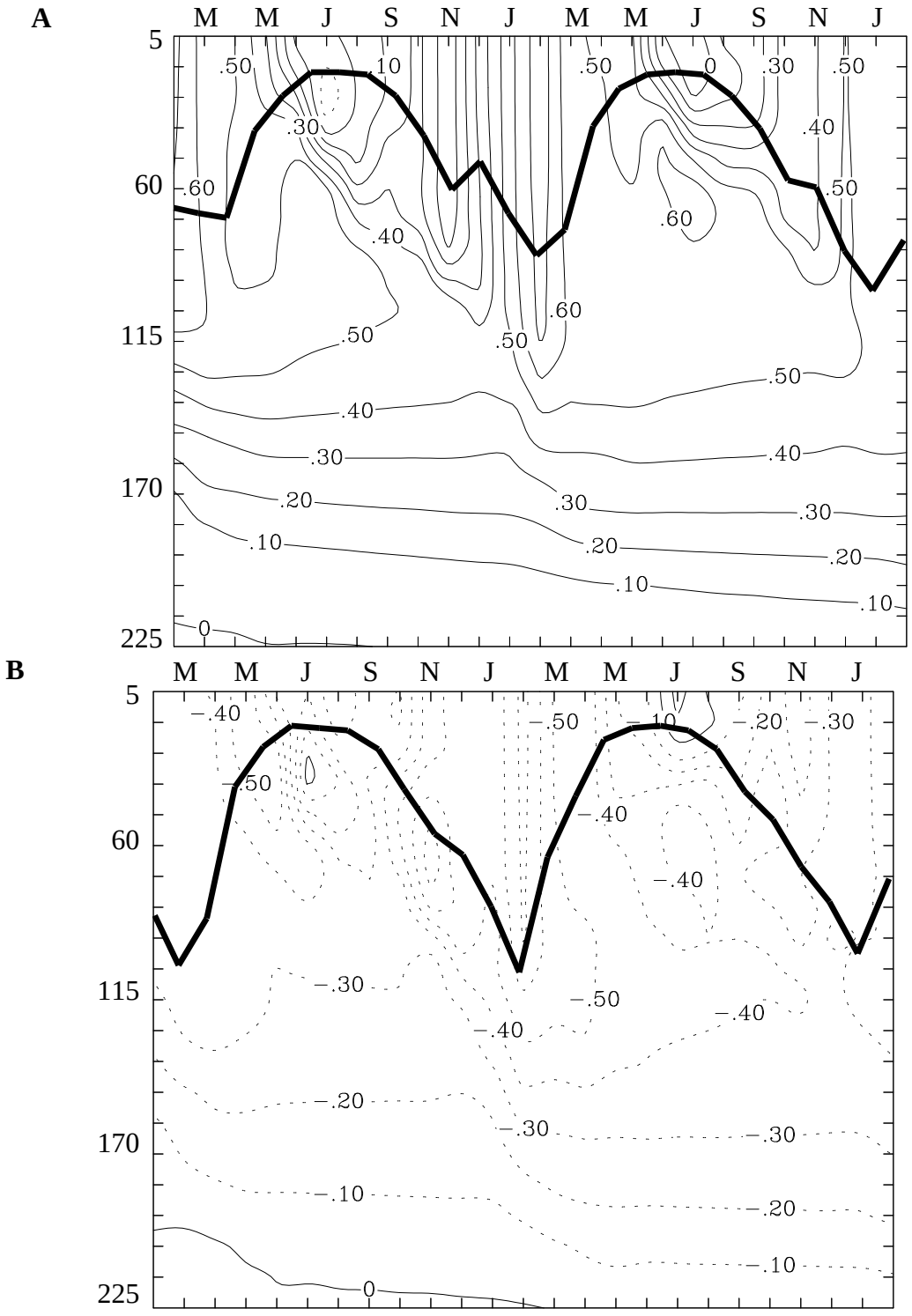

Figure 5-18. Composites ocean temperature anomalies with depth at the northern grid points for the a) warm and b) cold cases. Predicted mixed layer depth shown by bold line.

5.3 Role of Oceanic Entrainment in Persistence of Anomalies

5.3.1 Description of Sensitivity Experiments

A set of four uncoupled OWF experiments are presented that examine the influence of entrainment on the persistence of mixed-layer temperature anomalies. The mixed layer model is forced with daily heat fluxes, wind stress, and freshwater forcing (E-P; evaporation minus precipitation) from the 31 year coupled simulation. The role of variations of the entrainment forcing on the mixed layer temperature anomalies is investigated.

Weak damping (3 year time scale) in the ocean temperature tendency equation is necessary in these multi-year OWF simulations in order to prevent the ocean temperatures from drifting. If no damping is included then when the OWF experiments are forced with daily coupled simulation fluxes, the predicted temperatures drift. This drift is likely a result of machine truncation errors resulting from at least 2 numerical approximations of the coupled fluxes used to force the MLM in the OWF simulations. The communication between the ocean and the atmosphere in the coupled simulation takes place twice daily, and the fluxes were saved on the CCM1 history tapes once daily. Therefore, the OWF mixed layer model is not being forced with exactly the same heat fluxes as the coupled MLM. Additionally, the coupled simulation was integrated on a Cray YMP at NCAR, and the coupled fluxes are transferred to a workstation to perform the OWF simulations. The precision of the workstation is less than that of the supercomputer, which leads to a second source of error. Since the mixed layer model is highly nonlinear, particularly in OWF simulations, the small changes in surface forcing can lead the model predicted values to diverge greatly from the corresponding value in the coupled simulation. A damping time scale of 3 years was chosen in a trial and error manner in order that the persistence of the dipole mode in the OWF control closely resemble the coupled. A damping time scale of 3 years is significantly weaker than ‘actual’ values of damping 4-6 months (Frankignoul, 1985) inferred from the observations. If the coupled forcing terms were saved to machine precision, the model was forced with half daily fluxes, and the OWF simulations were integrated on the CRAY

YMP, then no damping would have been necessary in these OWF simulations. The 3 year damping time scale yields time coefficients of the dipole mode that display persistence and total variance (82% of coupled) reasonably close to that found in the fully coupled simulation. The total variance of mixed layer temperature is about 45% of the coupled in a OWF control experiment with a 6 month damping time scale. It is likely that a large portion of the reduction in variance of ocean temperatures in the OWF control simulation results from including the damping term. There is a good correspondence between the spatial patterns (Figure 5-19) and time coefficients (Figure 5-20) of EOF1 of mixed layer temperature in the coupled and the OWF control simulations.

The predictive equation for ocean temperature from the MLM is reviewed before the OWF experiments are described. The predictive equation for the mixed layer ocean temperature is:

$$\frac{\partial T_{mix}}{\partial t} = \frac{Q_{tot} - Q_{swh} + Q_{we}}{\rho_0 C_P h} + \frac{\nu_H}{h}\frac{\partial T_{mix}}{\partial z}\bigg|_{z = h} \qquad \textbf{(5-1)}$$

where T_{mix} is mixed layer ocean temperature, Q_{tot} total surface heat flux, Q_{swh} penetrating solar radiation, Q_{we} heating due to entrainment, ν_H eddy diffusivity, and h mixed layer depth. The first term on the right hand side of Equation 5-1 is the sum of the effects from heat fluxes at the atmosphere-ocean interface (Q_{tot}), penetrating through the bottom of the mixed layer (Q_{swh}), and the heat flux resulting from water entrained from below the mixed layer (Q_{we}). The second term on the right hand side of Equation 5-1 represents diffusion and is much smaller than the first term. The heating due to entrainment (Q_{we}) is given by:

$$Q_{we} = -w_e \cdot (T_{mix} - T_{below}) \cdot \rho_0 \cdot C_p \qquad \textbf{(5-2)}$$

here w_e is entrainment velocity, T_{below} the temperature below the mixed layer, ρ_0 the reference density of ocean water, and C_p the specific heat of ocean water. The term T_{dif} is defined as T_{mix} - T_{below}. When the mixed layer is deepening ($\frac{dh}{dt} > 0$) then:

$$w_e = \frac{dh}{dt} \qquad \textbf{(5-3)}$$

and when the mixed layer shallows then $w_e = 0$. Entrainment is inversely proportional to the difference between the temperature in the mixed layer and the layer below (T_{dif}), so entrainment tends to be smaller when the T_{dif} is larger. See Equations A9 to A12 in Appendix A for more details.

The Control (EXP1) is forced with daily total heat fluxes, wind stress, and E-P (evaporation minus precipitation) from the 31-year coupled simulation. The mixed layer temperatures are damped to climatology using a 3 year time scale, and the MLM predicts mixed layer temperature, depth, and salinity. In the sensitivity experiments (EXP2-4), the surface forcing and ocean temperature damping are identical to the control simulation, but the variability of entrainment heating is altered. A summary of the experiments is given in Table 5-1.

In EXP2, there are no anomalies in entrainment heating (Q_{we}') or mass flux which is achieved by specifying the annual cycle of mixed-layer depth and mean heating due to entrainment (Q_{we}) as the climatological values which are determined from EXP1. Comparing EXP2 with the control (EXP1) simulation will reveal the role of anomalous entrainment heating and mass flux on the ocean temperatures. In EXP1 and EXP2 the mean climatology of the mixed layer depths and entrainment heating (Q_{we}) is exactly the same by definition. Mixed layer temperatures in EXP2 drifted and were detrended before any processing was done.

EXP	Description	Comments	Process Isolated
OWF CON (EXP1)	Forced with heat, momentum, and freshwater fluxes from the coupled simulation. Ocean temperature is damped with 3-year time scale.	Serves as the control simulation.	
EXP2	Same forcing and damping as EXP1. The annual cycle of mean of h_{mix} and Q_{we} is specified. There are no anomalies in mixed layer depth (h_{mix}') and heating due to entrainment (Q_{we}').	Detrending of the data was necessary. Demonstrates the influence of anomalous entrainment heating on mixed layer temperatures.	$Q_{we}' = 0$ $h_{mix}' = 0$
EXP3	Same forcing and damping as EXP1. The submixed layer ocean temperatures are set to climatology on the first of each month from August (EXP2a) to Dec (EXP2e).	Stable simulation. Determines the time of year by when entrainment of the previous winter's deep ocean temperature anomalies has the largest impact on T_{mix}.	Set $T_{below}' = 0$
EXP4	Same forcing and damping as EXP1. Anomalies in the temperature difference between the mixed layer and the layer below are set to zero, $(T_{mix} - T_{below})' = 0$.	Stable simulation. Demonstrates the influence of anomalous temperature difference on T_{mix} and h_{mix}.	T_{dif} ' = 0

Table 5-1. A summary of the OWF experiments that are performed to examine the influence of entrainment on the persistence of ocean temperature anomalies.

In the series of sensitivity experiments 3a-e (EXP3a-EXP3e), the submixed layer temperatures are reset to the climatological values on first of each month starting with August and continuing to December, respectively. Comparing EXP3a to EXP1 will illuminate the role of anomalies stored below the mixed layer from the previous winter on mixed layer temperatures in the coming winter. Comparing EXP3a-3e will reveal the time of the year by when entrainment of subsurface anomalies from the previous winter have had their maximum impact on ocean temperatures. In these experiments there will also be some impact on mixed layer depth and entrainment heating when temperature anomalies from the previous winter are set to zero.

In EXP4, the temperature difference between the mixed-layer and the layer below (see Equation 5-2) is set to the climatological values (determined from EXP1) ($T_{dif}' = 0$) each day. Anomalies in ocean temperature associated with entrainment heating (Q_{we}') will oc-

cur from anomalous entrainment (w_e') as well as anomalies in mixed layer depth in this experiment. These experiments can reveal the impact on mixed layer depth, entrainment heating, and ocean temperatures when anomalies in the vertical temperature gradient between the mixed layer and the layer below the mixed layer are suppressed. Comparing EXP2 and EXP4 reveals how much of the impact of entrainment heating on mixed layer temperature in EXP2 is associated with the suppression of anomalies in the temperature difference between the mixed-layer and the layer below (T_{dif}) in EXP4.

5.3.2 Analysis

Monthly autocorrelations of mixed layer temperature in EXP2 and EXP1 (Figure 5-21) indicate that, without anomalies in entrainment heating, the persistence of ocean temperature is reduced. In EXP2, anomalies in mixed layer depth and its subsequent impact on SSTs are suppressed. In other climate studies, anomalies in mixed layer depth have been found to have a large impact on SSTs particularly during the summer months (Alexander and Penland, 1995).

Mixed layer temperature autocorrelations for EXP1 and EXP2 starting at all months are shown in Figure 5-22. The strong peak at a lag of 8-10 months associated with autocorrelations that begin in March seen in EXP1 is not present in the autocorrelations of EXP2. This supports the idea that anomalous heating from entrainment or 'Re-emergence' is responsible for significant autocorrelations in mixed layer temperature 9-10 months after March. The seasonal standard deviation in mixed layer temperature during fall (Figure 5-23a) is slightly larger in EXP2 than the control throughout the domain with the exception of the northwest part of the basin where the variance has decreased. The standard deviations ratios of EXP2 to EXP1 indicate that during winter (DJF) (Figure 5-23b) the variance is significantly larger in EXP2 than EXP1 throughout the basin. Recall that the variability of mixed layer depth is relatively small in the fall and is larger during winter (see Figure 4.8 c and d). Therefore, the impact of mixed layer depth anomalies is more likely to have a influence on mixed layer temperature variability during the winter rather than during the fall.

Variability in entrainment heating, which is large in the fall, could also lead to temperature tendency changes that impact wintertime mixed layer temperature anomalies.

In the OWF experiment 3 (a-e) series, the temperature anomalies below the mixed layer are set to zero each year on the first of the month going from August (experiment 3a) to December (experiment 3e). During August the mixed layer is relatively shallow and by resetting all sub-mixed anomalies to zero there is no carry over of sub-mixed layer temperature anomalies from one winter to the next. Monthly autocorrelations of mixed layer temperature for EXP3a, EXP3e, and EXP1 (Figure 5-24), indicate that the autocorrelations decay fastest in EXP3e, particularly at lags less than 24 months. The autocorrelations of mixed layer temperature starting at all months for EXP3a-e (Figure 5-25 a-e) indicate that the autocorrelation between one winter and the next gets larger as the reset date of the subsurface temperature anomalies is later. When the subsurface anomalies are reset on the first of December the mixed layer temperature autocorrelations (Figure 5-25e) between one winter and the next are still weaker than those from EXP1 (Figure 5-22a).

In the OWF experiment 4, the temperature difference between the mixed layer and the layer below is set to climatological values (T_{dif}' = 0) from the OWF control experiment (EXP1). The autocorrelations of mixed layer temperature in the northern part of the domain (Figure 5-26) decay faster than those in the control simulation. Monthly mixed layer temperature autocorrelations between one winter and the next are weak (Figure 5-25a) in EXP4. Mixed layer temperature variance is slightly larger in EXP4 than in the control during the winter season (not shown).

The results of EXP2 and EXP4 are very similar. The autocorrelations of mixed layer temperature based on all the months decay at a similar rate (compare Figure 5-22 and Figure 5-26). The autocorrelations of mixed layer temperature starting at all months for EXP2 and EXP4 are also similar (compare Figure 5-22 and Figure 5-27). The similarity of EXP2 and EXP4 suggests that anomalies in T_{dif} are an important component of anomalies in entrainment heating (Q_{we}) associated with the 'Re-emergence' mechanism. It is likely

that anomalies in entrainment velocity (w_e) are of secondary importance compared to those in T_{dif} in the formation of entrainment heating anomalies.

Limiting the variability of entrainment in the MLM, whether by setting subsurface anomalies to zero or specifying climatological values of heating due to entrainment and mixed layer depths, has had the most notable effect of reducing persistence of mixed layer temperatures on interannual time scales for the dipole mode of variability.

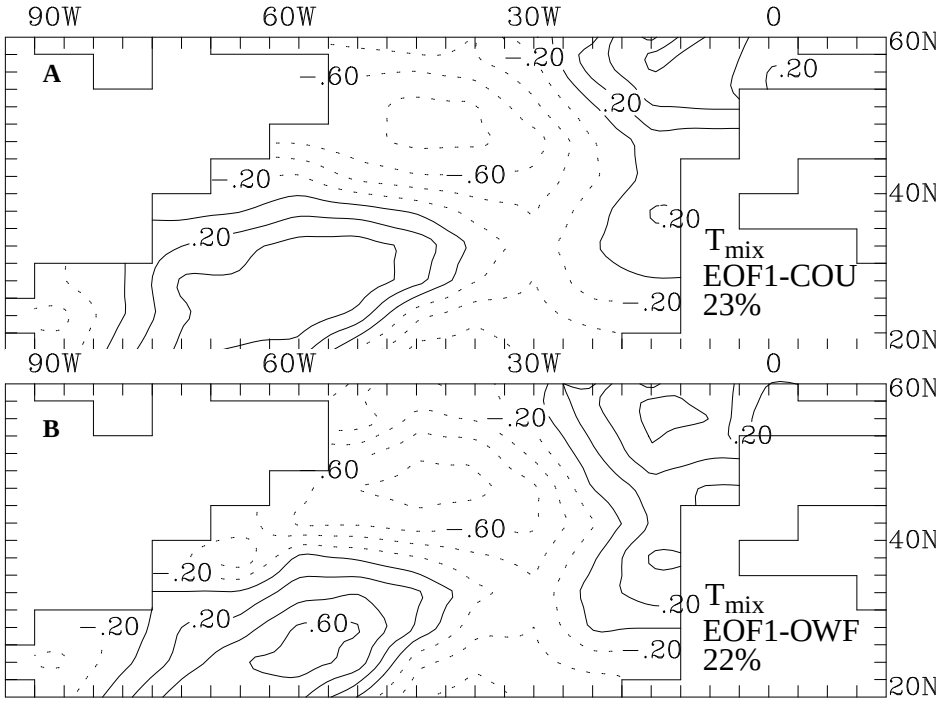

Figure 5-19. EOF1 of wintertime (averaged over DJF) mixed layer temperature in the (a) coupled and (b) OWF control simulations explain 23% and 22% of the total variance, respectively. The EOFs are shown as correlations between their respective time coefficients and the full mixed layer temperature data.

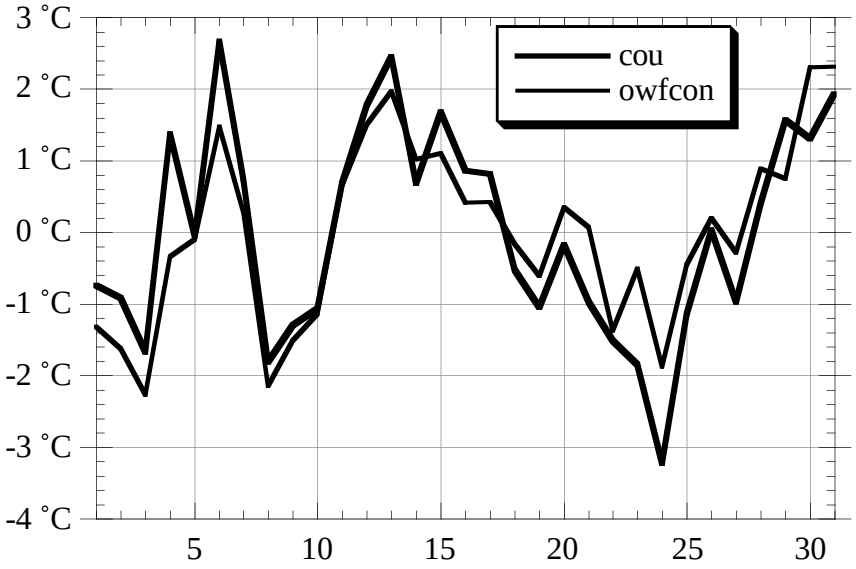

Figure 5-20. Time coefficients from EOF1 (dipole mode) of mixed layer temperature in ˚C from the coupled (thick line) and OWF control (thin line) simulations.

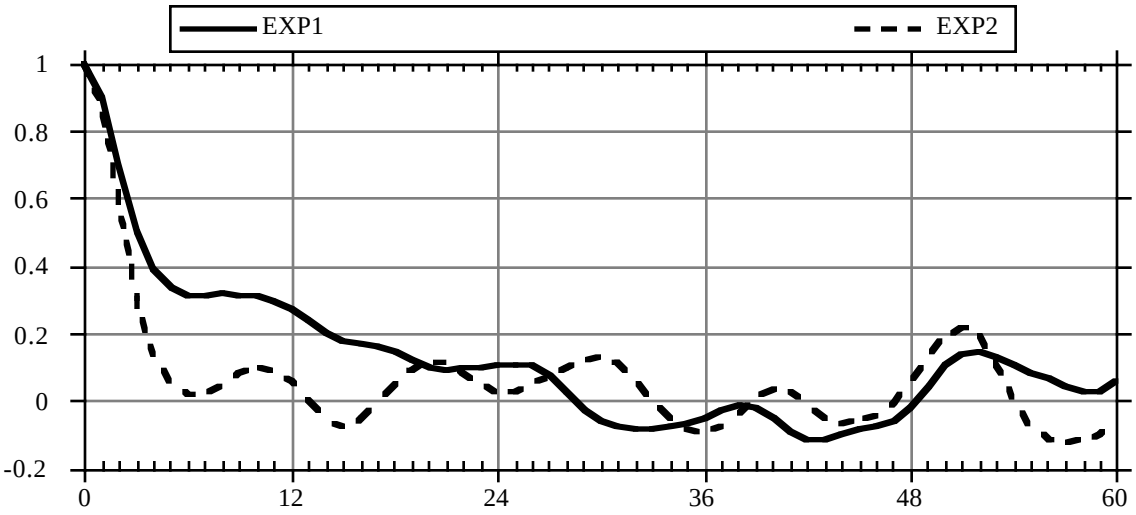

Figure 5-21. Monthly autocorrelations of T_{mix} averaged over the northern center of the dipole mode of variability for EXP2 and the control (EXP1).

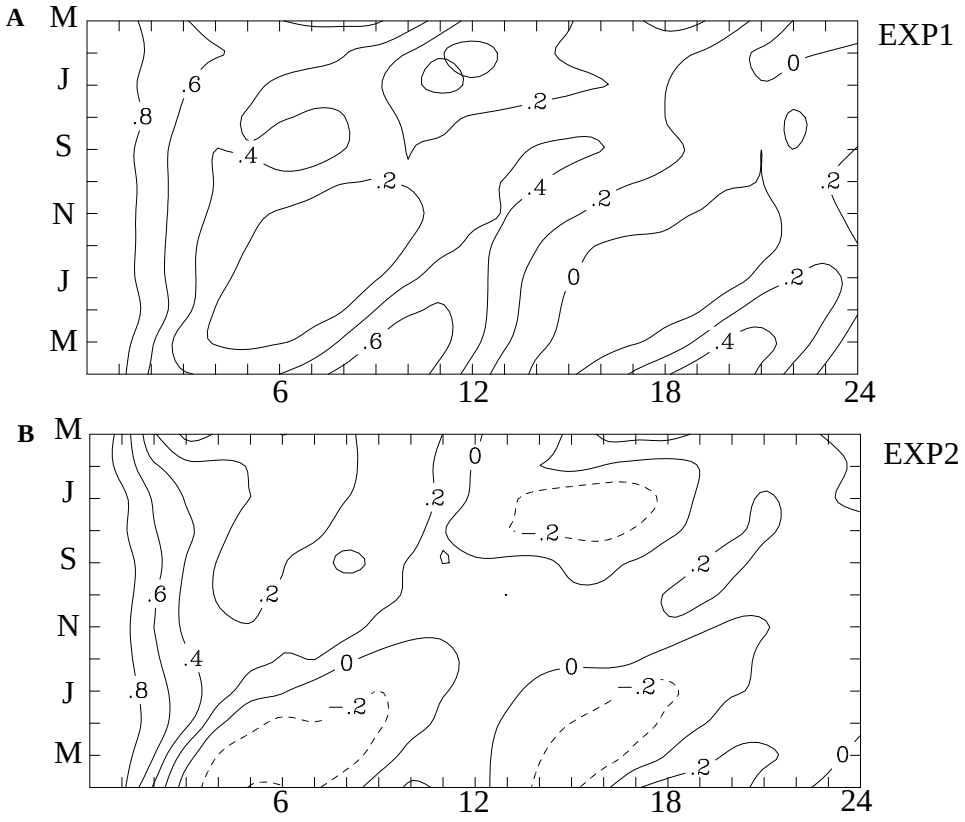

Figure 5-22. Autocorrelations of T_{mix} averaged over the northern grid points centered at the maximum variance for the dipole mode of variability for a) EXP1 and b) EXP2 at monthly lags of 0 to 24.

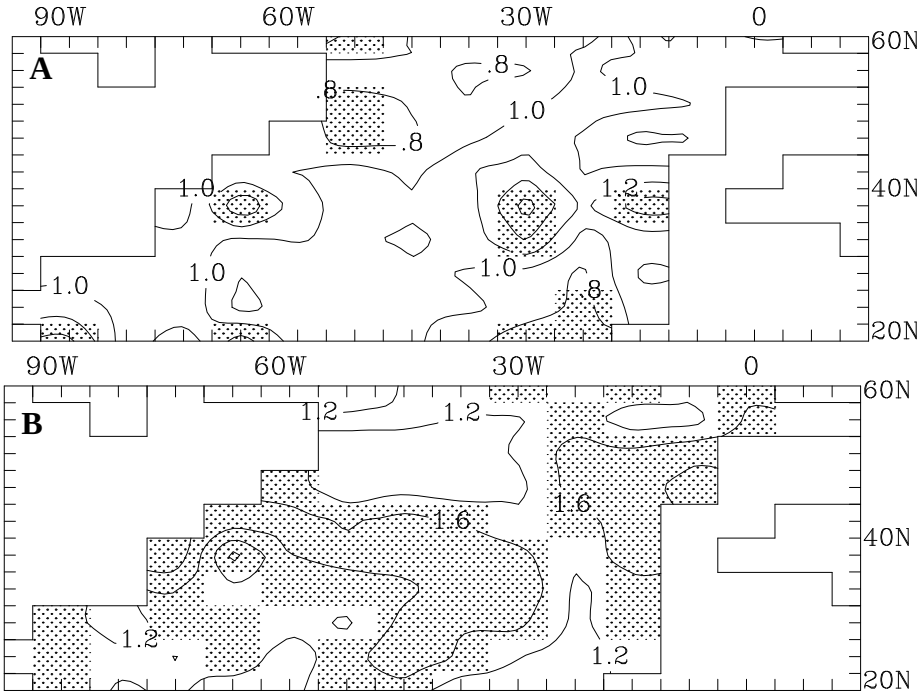

Figure 5-23. Ratio of seasonally averaged T_{mix} standard deviation ratio of EXP2 over EXP1 during a) SON and b) DJF. Statistical significance at the 95% level or greater using an ftest is indicated by shading.

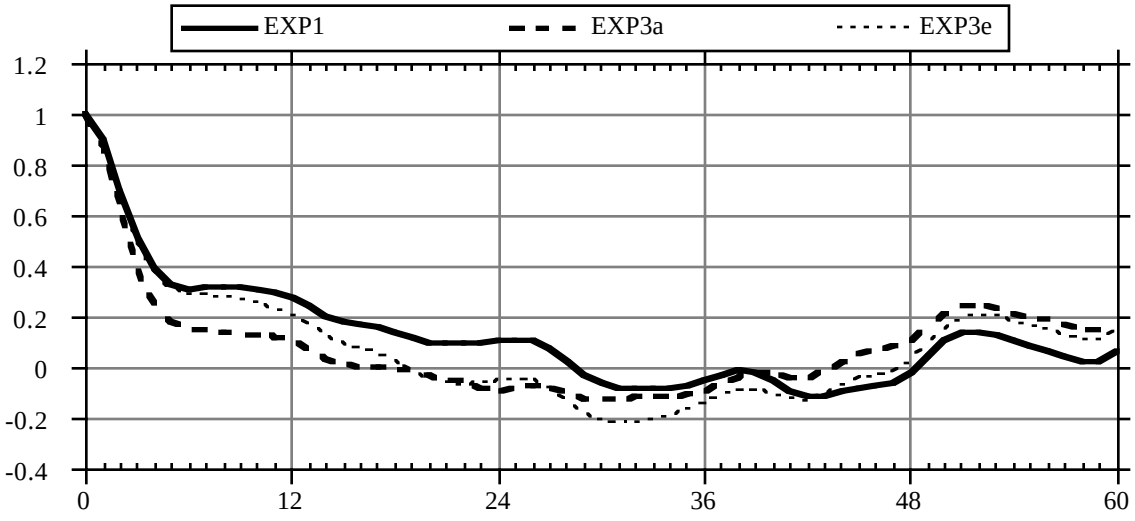

Figure 5-24. Monthly autocorrelations of T_{mix} averaged over the northern center of the dipole mode of variability for EXP3a, EXP3e, and the control (EXP1).

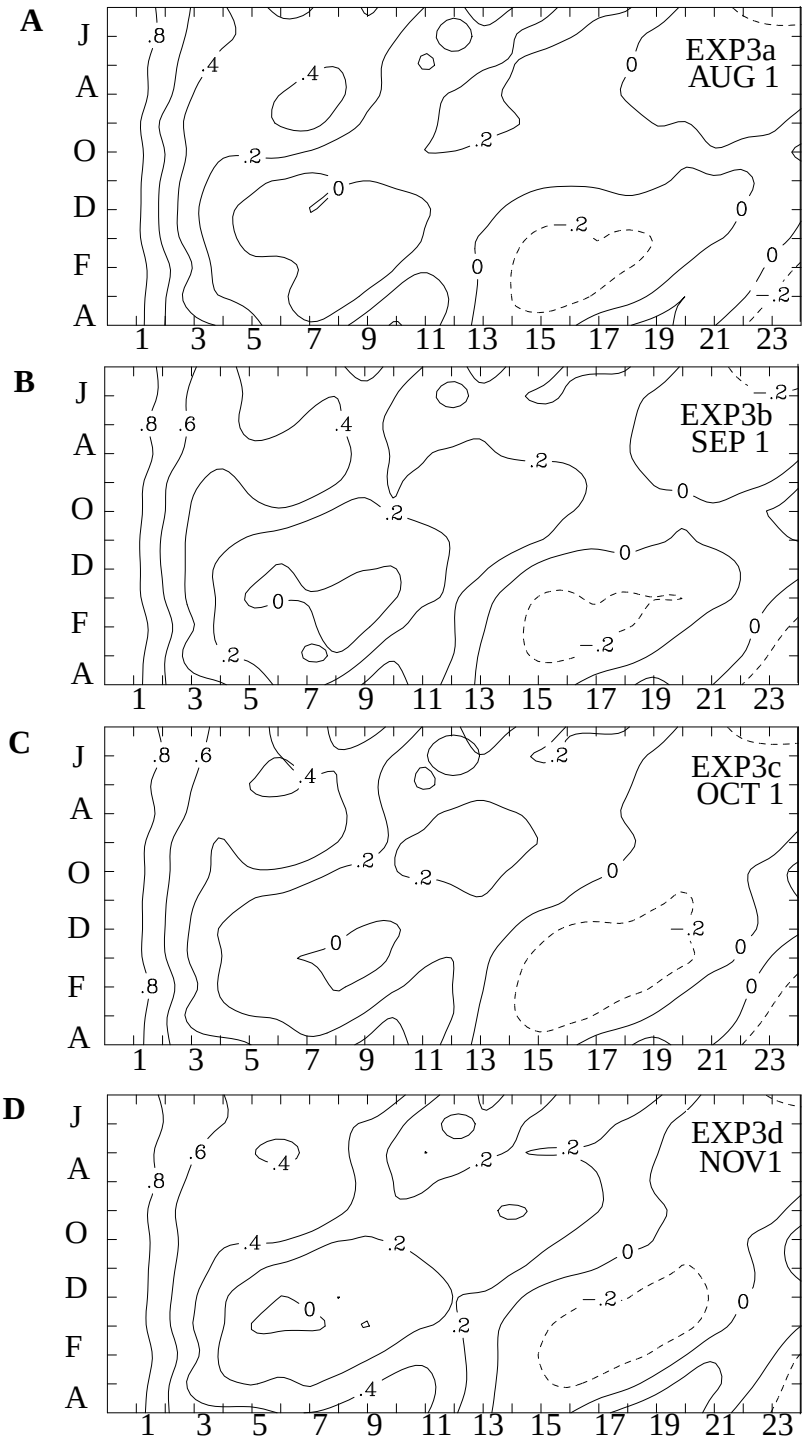
A
B
C
D
J
A
O
D
F
A
EXP3a
AUG 1
EXP3b
SEP 1
EXP3c
OCT 1
EXP3d
NOV1
1 3 5 7 9 11 13 15 17 19 21 23

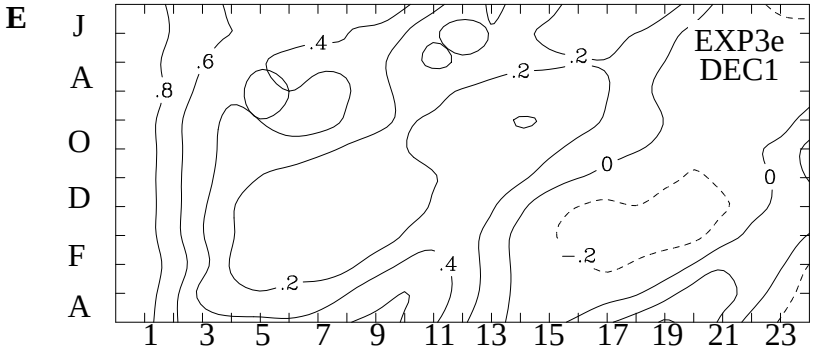

Figure 5-25. Monthly autocorrelations of T_{mix} in the north for a) EXP3a, b) EXP3b, c) EXP3c, d) EXP3d, and e) EXP3e. The starting months are shown on the ordinate.

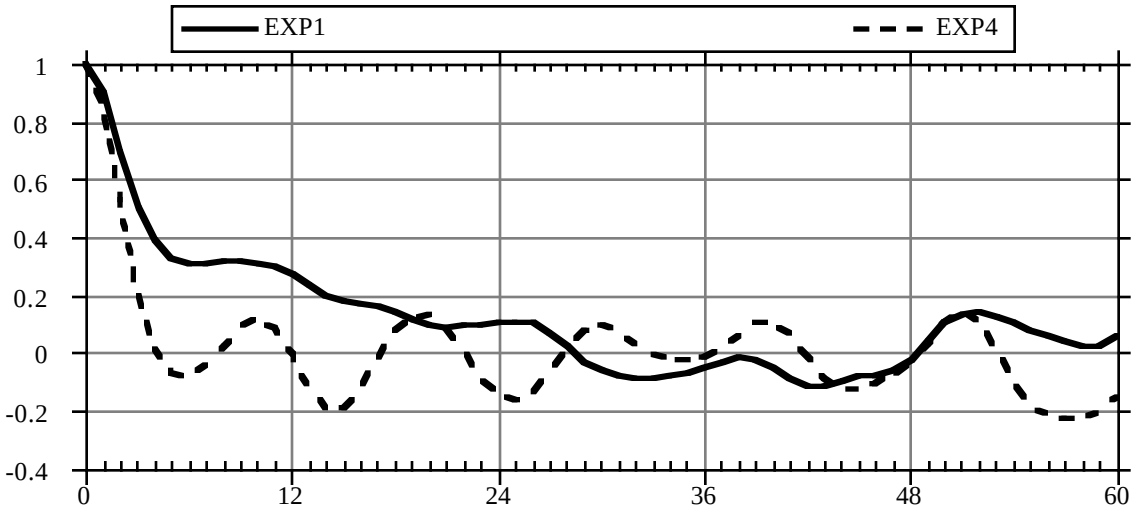

Figure 5-26. Monthly autocorrelations of T_{mix} averaged over the northern center of the dipole mode of variability for EXP4 and the control (EXP1).

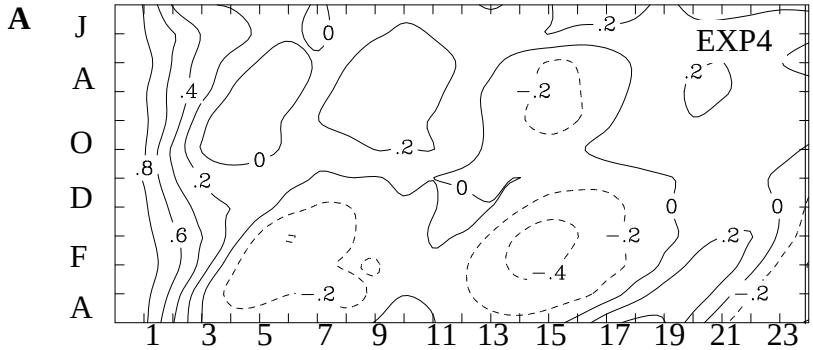

Figure 5-27. Monthly autocorrelations of T_{mix} in the north for EXP4. The starting months are shown on the ordinate.

5.4 Summary

The persistence of air temperature anomalies from one winter to the next, as seen in increased autocorrelations of the time coefficients of EOF1 of air temperature between the coupled and the control simulations, is associated with persistence of ocean temperature anomalies. Ocean temperature anomalies during late winter penetrate deep into the ocean, since the mean mixed layer depths are maximum at this time of year. The stable summer mixed layer reforms close to the surface layer, decoupling the deeper ocean from the atmosphere. Anomalies in ocean temperature associated with the previous winter remain intact below the summer thermocline. In the fall the mixed layer deepens and the anomalous temperatures are reincorporated into the mixed layer.

The 'Re-emergence' mechanism is clearly evident in the northern center of the dipole mode of variability. Anomalies in ocean temperature that are associated with the Re-emergence mechanism in the coupled simulation clearly have an impact on air temperatures. This is evident in the autocorrelations of air and ocean temperatures (compare Figure 5-6b and Figure 5-8a). The impact of the ocean on the atmosphere is noteworthy since the literature is divided on whether or not the midlatitude ocean has any influence on the northern hemispheric atmosphere. When entrainment anomalies are suppressed in the MLM (as in EXP2) the large autocorrelations in ocean temperature between one winter and the next disappear. An analysis of sub-mixed layer ocean temperature anomalies also shows that 'Re-emergence' plays an important role in the northern part of the basin.

The 'Re-emergence' mechanism is stronger in the model than the observations because of the one-dimensional structure of the ocean model. Autocorrelations of ocean surface temperature are significant up to a lag of 24 months (Figure 5-8a) in the model, which is not true in the observations (Figure 5-8c). Advective effects in the ocean will act to reduce the impact of the re-emergence of anomalies through the mixing of sub-mixed layer temperature anomalies.

Coupling also leads to an increase in the persistence of air temperature anomalies on the time scale of several months throughout the ocean basin. This increase in persistence of

air temperature anomalies, together with the increase in variance of air temperature and the decrease in variance of heat flux suggests that coupling leads to a decrease of damping of air temperature anomalies by heat fluxes (decreased ‘Thermal Damping’, Barsugli 1995). These effects are most noticeable in the coupled model during the warmer summer months.